

The present work was submitted to
Institute for Communication Technologies and Embedded Systems (ICE)
RWTH Aachen University

Prof. Dr. Haris Gačanin

Prof. Dr. rer. nat. Rainer Leupers

Master's Thesis FIXME: DSP-/ISS-/SSS-INTERNAL NUMBER

ANALYSIS OF MULTI-USER UPLINK CHANNEL
WITH MIMO

ANALYSE EINES
MEHRBENUTZER-MEHRFACHZUGRIFFSKANALS
MIT MIMO

by

HELENA PUJOLAR BASTIAN

Matr.-No. 448066

MARCH 2023

Supervisors:

Prof. Dr. Haris Gačanin

Prof. Dr. Ana Isabel Pérez Neira

Dr. Kenan Turbic

This document is for internal use only.
All copyrights are controlled by the supervising chair at RWTH Aachen.
Publications of any kind must be authorized.

Eidesstattliche Versicherung

Statutory Declaration in Lieu of an Oath

Pujolar Bastian, Helena

448066

Name, Vorname/Last Name, First Name

Matrikelnummer (freiwillige Angabe)

Matriculation No. (optional)

Ich versichere hiermit an Eides Statt, dass ich die vorliegende Arbeit/Bachelorarbeit/
Masterarbeit* mit dem Titel

I hereby declare in lieu of an oath that I have completed the present paper/Bachelor thesis/Master thesis* entitled

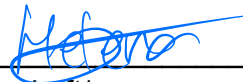
Analysis of Multi-User Uplink Channel with MIMO

selbstständig und ohne unzulässige fremde Hilfe (insbes. akademisches Ghostwriting) erbracht habe. Ich habe keine anderen als die angegebenen Quellen und Hilfsmittel benutzt. Für den Fall, dass die Arbeit zusätzlich auf einem Datenträger eingereicht wird, erkläre ich, dass die schriftliche und die elektronische Form vollständig übereinstimmen. Die Arbeit hat in gleicher oder ähnlicher Form noch keiner Prüfungsbehörde vorgelegen.

independently and without illegitimate assistance from third parties (such as academic ghostwriters). I have used no other than the specified sources and aids. In case that the thesis is additionally submitted in an electronic format, I declare that the written and electronic versions are fully identical. The thesis has not been submitted to any examination body in this, or similar, form.

Aachen, 28th March 2023

Ort, Datum/City, Date



Unterschrift/Signature

*Nichtzutreffendes bitte streichen

*Please delete as appropriate

Belehrung:

Official Notification:

§ 156 StGB: Falsche Versicherung an Eides Statt

Wer vor einer zur Abnahme einer Versicherung an Eides Statt zuständigen Behörde eine solche Versicherung falsch abgibt oder unter Berufung auf eine solche Versicherung falsch aussagt, wird mit Freiheitsstrafe bis zu drei Jahren oder mit Geldstrafe bestraft.

Para. 156 StGB (German Criminal Code): False Statutory Declarations

Whoever before a public authority competent to administer statutory declarations falsely makes such a declaration or falsely testifies while referring to such a declaration shall be liable to imprisonment not exceeding three years or a fine.

§ 161 StGB: Fahrlässiger Falscheid; fahrlässige falsche Versicherung an Eides Statt

(1) Wenn eine der in den §§ 154 bis 156 bezeichneten Handlungen aus Fahrlässigkeit begangen worden ist, so tritt Freiheitsstrafe bis zu einem Jahr oder Geldstrafe ein.

(2) Straflosigkeit tritt ein, wenn der Täter die falsche Angabe rechtzeitig berichtigt. Die Vorschriften des § 158 Abs. 2 und 3 gelten entsprechend.

Para. 161 StGB (German Criminal Code): False Statutory Declarations Due to Negligence

(1) If a person commits one of the offences listed in sections 154 through 156 negligently the penalty shall be imprisonment not exceeding one year or a fine.

(2) The offender shall be exempt from liability if he or she corrects their false testimony in time. The provisions of section 158 (2) and (3) shall apply accordingly.

Die vorstehende Belehrung habe ich zur Kenntnis genommen:

I have read and understood the above official notification:

Aachen, 28th March 2023

Ort, Datum/City, Date



Unterschrift/Signature

Acknowledgments

I would like to express my deepest appreciation to Prof. Dr. Ana Isabel Pérez Neira and Prof. Haris Gačanin for giving me the opportunity to work with them and provide their knowledge and expertise. I am also grateful to Dr. Kenan Turbic for his invaluable advice and patience.

I would like to thank all my colleagues for their support and warm welcome to the institute. My sincere thanks to my friends in Aachen for making this experience far more than enjoyable.

Lastly, I would like to thank my family for their continuous support. Especially to my father and Laura for their encouragement and for always being there. And to you, mom, for believing in me even when I did not. Wherever you are, I will be forever grateful.

Abstract

The increasing number of connected users as well as the availability of new services and mobile applications drive the need for higher data rates. In order to fulfill such expectations different strategies such as spatial multiplexing have been introduced. This thesis is centered on the Multi-User Uplink Channel where different users transmit to a single base station with multiple antennas.

The purpose of this thesis is to design the transmitter and the receiver architectures so that the maximum sum rate of a Multi-User Uplink Channel reaches the capacity for single and multi-antenna users. In the literature there is a lack of practical implementations and not many studies exploit the multi-antenna user scenario. It is important to properly characterize the capacity region and define practical implementation schemes on the uplink direction to design the architecture for the Multi-User Downlink Channel also referred as the Broadcast Channel, which is a more complex problem based on the uplink solution.

The design of the optimal transmitter is motivated by the analysis of capacity first for the single user scenario with Multi Input Multi Output Peer-to-Peer (MIMO P2P) communications followed by the Multi-User scenario for single and multi-antenna users. At the receiver three types of beamformers are analyzed and compared: Zero Forcing, QR and Minimum Mean Squared Error beamformer. Results for the Bit Error Rate performance and maximum sum rate for the different receivers are provided.

The thesis results show that the optimal architecture for the Multi-User Uplink with multi-antenna users that achieves capacity is the combination of the optimal MIMO P2P design, based on the Singular Value Decomposition of the channel matrix and the Water Filling power allocation. For the receiver part the Minimum Mean Squared Error beamformer is proven to achieve capacity. Channel State Information is needed at the transmitter and receiver, therefore a channel estimation algorithm is provided based on orthogonal sequences and is proven to deliver good Bit Error Rate results.

Contents

1	Introduction	3
1.1	Background and Motivation	3
1.2	State of the Art	4
1.3	Summary and Conclusions	5
2	System model	7
2.1	Introduction to multi-antenna systems	7
2.1.1	Capacity	8
2.1.2	No CSI at the TX	9
2.1.3	CSI at the TX	9
2.2	MU-UL with single-antenna UEs	11
2.3	MU-UL with multi-antenna UEs	11
2.4	Architecture design	12
2.4.1	Single-antenna UE	12
2.4.2	Multi-antenna UEs	21
3	Performance analysis	27
3.1	Simulator implementation	27
3.1.1	Pseudocode	27
3.1.2	Flow chart	28
3.2	SISO	28
3.2.1	Gaussian channel	28
3.2.2	Rayleigh fading channel	29
3.2.3	Capacity analysis	30
3.3	MIMO P2P	31
3.4	MU-UL with single-antenna UEs	33
3.5	MU-UL with multi-antenna UEs	36
4	Channel estimation	39
4.1	Pilot symbols transmission	39
4.2	Pilot sequence generation for multi-antenna system	39

5	Conclusions	47
A	SVD decomposition	49
B	Central Limit Theorem	51
C	Minimum Mean Square Error Estimator	53
D	Detection in Gaussian Noise	55
	List of Figures	60
	References	61

Abbreviations

AWGN Additive **W**hite **G**aussian **N**oise
BER Bit **E**rror **R**ate
BS Base **S**tation
CE Channel **E**stimation
CFR Channel **F**requency **R**esponse
CIR Channel **I**mpulse **R**esponse
CLT Central **L**imit **T**heorem
CRB Cramer **R**ao **B**ound
CSI Channel **S**tate **I**nformation
CSIR Channel **S**tate **I**nformation at the **R**eceiver
CSIT Channel **S**tate **I**nformation at the **T**ransmitter
DD Direct **D**ecision
DL Down **L**ink
EVD Eigen **V**alue **D**ecomposition
FDD Frequency **D**ivision **D**uplexing
HW Hard **W**are
IEEE Institute of **E**lectrical and **E**lectronics **E**ngineers
ISI Inter **S**ymbol **I**nterference
LMMSE Linear **M**inimum **M**ean **S**quared **E**rror
LS Least **S**quare
MAC Multiple **A**ccess **C**hannel
ML Maximum **L**ikelihood
MIMO Multiple **I**nput **M**ultiple **O**utput
MISO Multiple **I**nput **S**ingle **O**utput
MU-UL Multiple **U**ser **U**plink
MRC Maximal **R**atio **C**ombining
MSE Minimum **S**quared **E**rror
MMSE Minimum **M**ean **S**quared **E**rror
OFDM Orthogonal **F**requency **D**ivision **M**ultiplexing
PA Pilot **A**ssisted
PAPR Peak to **A**verage **P**ower **R**atio
P2P Peer to **P**eer
RF Radio **F**requency
QAM Quadrature **A**mplitude **M**odulation
RX Receiver
SC Single **C**arrier
SDMA Space **D**ivision **M**ultiple **A**ccess
SER Symbol **E**rror **R**ate
SIC Signal **I**nterference **C**anceller
SIMO Single **I**nput **M**ultiple **O**utput
SINR Signal to **I**nterference plus **N**oise **R**atio

SNR Signal to Noise Ratio
SISO Single Input Single Output
SNR Signal to Noise Ratio
SVD Singular Value Decomposition
SW Soft Ware
TDD Time Division Duplexing
TX Transmitter
UE User Equipment
UL Up Link
UPA Uniform Power Allocation
WCDMA Wideband Code Division Multiple Access
WF Water Filling
WLAN Wireless Local Area Network
ZF Zero Forcer
ZMCSCG Zero Mean Circularly Symmetric Complex Gaussian

1 Introduction

1.1 Background and Motivation

Since the beginning of wireless communications, the increasing number of connected users as well as the availability of new services and mobile applications drive the need for higher data rates. In order to fulfill such expectations different generations of mobile communications systems have been standardized. Fifth Generation (5G) is the latest being implemented in practical systems while research is already being conducted in order to define the 6th Generation.

The need to fulfill this high data rate demand impulsed the development of multiplexing techniques and diversity schemes among others. This thesis is centered on spatial multiplexing where the receiver (RX) and the transmitter (TX) consist of multiple antennas which is known as Multiple Input Multiple Output (MIMO) communications.

In Single Input Single Output (SISO) schemes where the TX and RX consist of one antenna, the data rate can be increased by either increasing the transmission bandwidth or the power. This can be directly derived from Shannon's channel capacity formula

$$C = B \log_2(1 + \rho) \quad (1.1)$$

where B is the bandwidth and ρ the signal-to-noise-ratio (SNR). Both bandwidth and power are limited resources that cannot be arbitrarily increased. Moreover, in interference-limited systems, a higher transmission power of one user results in increased interference for users. For a SISO system, the spectral efficiency is limited by the power in bandwidth. In MIMO systems, spectral efficiency can be increased by using multiple antennas at the TX and the RX, without increasing the power or the bandwidth. Basically, two fundamental gains are achieved in MIMO:

1. *Rate gain*: is the increase in the achievable data rate of a MIMO system compared to the SISO one by sending different information at every TX antenna. It is also known as the multiplexing gain and it is in the focus of this thesis.
2. *Diversity gain*: instead of sending different data, the same information is sent to all TX antennas, the data experiences different paths, and the RX can benefit from that and decode the data with higher reliability.

Rate and diversity gain are both related to the channel matrix rank. The maximum rank of a channel matrix is the minimum between the number of TX and RX antennas. This corresponds to the number of independent spatial modes or paths over which data can be transmitted.

When referring to MIMO, one usually thinks of Peer-to-Peer (P2P) communications but this thesis goes beyond this single-user scenario and also considers a multi-user case where different users equipment (UEs) with single or multiple antennas transmitting to a single RX, the base station (BS). This is known as the Multiple Access Channel (MAC) or the Multi-User Uplink Channel (MU-UL), not to be confused with the MAC layer of the communication protocol stack.

When multiple users simultaneously transmit, the RX needs to focus in different directions to get the proper information from every user, i.e., beamforming. The RX can implement different beamformers to cancel or attenuate the interference between UEs. The performance of the overall communication system, among other considerations, will also be affected by the beamformer implemented.

The motivation to write this thesis comes from the need to characterize practical systems for the MU-UL. Many studies put an effort into the analysis of capacity expressions, but a few explain in detail its practical implementation. Moreover, the number of works devoted to MU-UL with multi-antenna UEs is significantly lower compared to the single-antenna case. It is important to properly characterize the MU-UL capacity region and define practical implementation schemes to design the TX and RX architecture for the Multi-User Downlink Channel (MU-DL) also referred as the Broadcast Channel (BC) in the literature. A remarkable contribution to the existent works is the mapping from the MU-UL beamforming matrix to the MU-DL in [1].

1.2 State of the Art

The MIMO communications started with antenna diversity, whose roots began in the 1920s, with RCA engineers Harold H. Beverage and Harold O. Foschini showed the communication capacity by a system with $N_T \times N_R$ antennas assuming that the TX does not have the Channel State Information (CSI) and he introduced the V-BLAST (Vertical-Bell Laboratories Layered Space-Time) detection algorithm for MIMO systems. Alamouti proposed a transmit diversity scheme that provided optimal precoding to exploit multipath properties when the TX does not have CSI (NO-CSI) [2]. A lot of work has been devoted to analyzing the characteristics of \mathbf{H} to take advantage of multipath propagation. Apart from the study of \mathbf{H} , much effort has been dedicated to the design of compact MIMO antennas to offer strong performance in a variety of environments, without suffering large degradation due to strong antenna mutual coupling.

A new challenge arises when having decentralized communication schemes either at the TX or the RX. This thesis focuses on the MU-UL channel where TXs do not cooperate when transmitting to a single RX. The study of the MU-UL dates back to the days of Shannon [3]. Meanwhile, the MU-DL, was first introduced by Cover in the 1970s [4]. Many existent works study the capacity of the MU-UL as well as the MU-DL, but there are not many works describing its practical implementation to achieve these capacities. In [5], the author analyses the MU-UL channel capacity and with the duality concept extends the study to the DL. For the DL direction the author considers both the Additive White Gaussian Noise (AWGN) channel and Rayleigh fading, but for the UL direction only results for the AWGN are provided. Moreover, its focus is on capacity analysis rather than the practical implementation. Another work devoted to the MU-UL is [6], where the author focuses on the capacity for multi-antenna UEs in the particular case of AWGN channel.

The study in [7] provides a wide study of MU-UL with multi-antenna UEs for fading channels which includes expressions for the MU-UL and MU-DL capacity. It also gives expressions for the beamforming techniques at the RX, similar to the ones studied in this thesis.

This thesis analyzes the maximum sum rate of different practical systems. The major contribution of this work is the implementation and validation of a simulator for MU-UL with multi-antenna UEs. The optimal capacity-achieving beamformer RX Minimum Mean Squared Error (MMSE) is studied and compared against suboptimal beamformers, such as Zero Forcing (ZF) [8] and QR [9].

Related works like [10] present a performance analysis of the MU-UL techniques comparing the ZF RX and the Maximum Ratio Combining (MRC) for the single-antenna case. The study in [11] analyzes the cell throughput performance of MU-UL with multi-antenna UEs for the ZF and MMSE beamformer. Also, in [12] the throughput of a multi-cell MU-UL channel with single-antenna UEs is analyzed with a ZF RX.

1.3 Summary and Conclusions

The purpose of this thesis is to design the TX and RX architectures so that the maximum sum rate of a MU-UL channel reaches the capacity for single and multi-antenna UEs. In particular, three types of beamformers are analyzed and compared: Zero Forcing (ZF), QR and Minimum Mean Squared Error (MMSE) beamformer.

The thesis results show that the optimal architecture of the RX which achieves capacity is the combination of the optimal MIMO P2P design and the MMSE beamformer in MU-UL channel. Channel State Information (CSI) is needed at the TX and RX, therefore a channel estimation (CE) algorithm is provided based on orthogonal sequences.

The organization of this thesis is the following. Chapter 2 presents the theoretical background based on MIMO P2P, follows by describing the system model for MU-UL with single and multi-antenna UEs. In both cases, the capacity is studied first to motivate the design of the TX that follows. Afterward, the three different beamformers are presented. Chapter 3 starts with a pseudocode and a flow chart of the developed SW simulator. Then it presents the performance analysis based on the bit error rate (BER) and compares the sum rate and capacity for the different beamformers. For software (SW) simulation model development and validation first the SISO system is studied, followed by MIMO P2P and finally the MU-UL system for single and multi-antennas UEs is considered. Chapter 4 describes the implementation of a CE algorithm based on orthogonal sequences for multi-antenna systems. Finally, Chapter 5 outlines the conclusions and presents future work.

2 System model

2.1 Introduction to multi-antenna systems

The simplest hardware device for a TX and RX includes just one antenna at every communications side. The link between two devices with this characteristic is named SISO, with the following representation in Figure 2.1. The RX needs to estimate only one channel coefficient between the TX and RX.

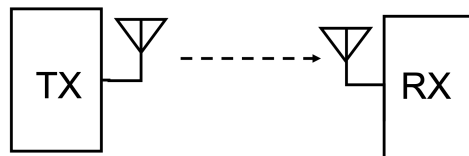


Figure 2.1: SISO.

When the RX consists of more than one antenna at his side (spatial diversity), and the TX has no diversity, the link is named Single Input Multiple Output (SIMO). The RX in Figure 2.2 uses the information received from both antennas, and after the combiner matrix block, the system improves its performance, i.e. it achieves lower BER.

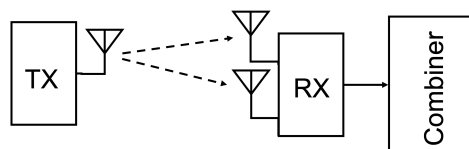


Figure 2.2: SIMO.

In the case of diversity on the TX side, a precoder block is necessary for transmission when the total number of antennas on both sides is different. Figure 2.3 presents a scheme of the system.

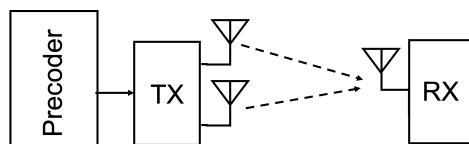


Figure 2.3: MISO.

Combining the last two scenarios, the MIMO P2P (2.4) communications system is achieved with diversity at both the TX and RX.

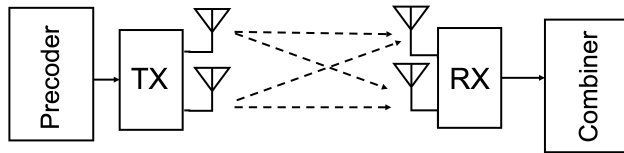


Figure 2.4: MIMO.

2.1.1 Capacity

The capacity of the MIMO system is the maximum error-free data rate that a channel can support [13]. The received signal \mathbf{y} between the N_T TX and N_R RX antennas is:

$$\mathbf{y} = \sqrt{\frac{E_s}{N_T}} \mathbf{H} \mathbf{x} + \mathbf{n} \quad (2.1)$$

where \mathbf{y} is the $N_R \times 1$ RX signal vector, \mathbf{x} is the $N_T \times 1$ TX one, \mathbf{n} is the AWGN noise with covariance matrix $E(\mathbf{n}\mathbf{n}^H) = N_0 \mathbf{I}_{N_R}$ and E_s is the total average TX energy. The covariance matrix of \mathbf{x} is $\mathbf{R}_{xx} = E(\mathbf{x}\mathbf{x}^H)$ that is assumed to have zero mean and the trace (Tr) of the covariance matrix $\text{Tr}(\mathbf{R}_{xx}) = N_T$ constrains the total average energy transmitted over a symbol period.

For this first analysis CSI will be assumed at the RX, and \mathbf{H} will be treated as deterministic. The capacity of the MIMO channel is defined as

$$C = \max_{f(\mathbf{x})} I(\mathbf{x}; \mathbf{y}) \quad (2.2)$$

where $f(\mathbf{x})$ is the probability distribution function of the vector \mathbf{x} and $I(\mathbf{x}; \mathbf{y})$ is the mutual information between vectors \mathbf{x} and \mathbf{y} . By the definition:

$$I(\mathbf{x}; \mathbf{y}) = H(\mathbf{y}) - H(\mathbf{y}|\mathbf{x}) \quad (2.3)$$

where $H(\mathbf{y})$ is the differential entropy of the vector \mathbf{y} and $H(\mathbf{y}|\mathbf{x})$ the conditional differential entropy of the vector \mathbf{y} when \mathbf{x} is known. Since \mathbf{x} and \mathbf{n} are independent, $H(\mathbf{y}|\mathbf{x}) = H(\mathbf{n})$ and (2.3) simplifies to:

$$I(\mathbf{x}; \mathbf{y}) = H(\mathbf{y}) - H(\mathbf{n}) \quad (2.4)$$

Maximizing mutual information in (2.2) is equivalent to maximizing $H(\mathbf{y})$ that is maximized when \mathbf{y} is Zero-Mean Circularly Symmetric Complex Gaussian (ZMCSCG) [13]. The covariance matrix of \mathbf{y} , $\mathbf{R}_{yy} = E(\mathbf{y}\mathbf{y}^H)$, satisfies:

$$\mathbf{R}_{yy} = \frac{E_s}{N_T} \mathbf{H} \mathbf{R}_{xx} \mathbf{H}^H + N_0 \mathbf{I}_{N_R} \quad (2.5)$$

The previous condition that \mathbf{y} must be ZMCSCG implies that \mathbf{x} must be a ZMCSCG vector, the distribution of which is completely characterized by \mathbf{R}_{xx} . The differential entropy of vectors \mathbf{y} and \mathbf{n} are given by:

$$H(\mathbf{y}) = \log_2(\det(\pi e \mathbf{R}_{yy})) \quad (2.6)$$

$$H(\mathbf{n}) = \log_2(\det(\pi e N_0 \mathbf{I}_{N_R})) \quad (2.7)$$

Therefore, $I(\mathbf{x}; \mathbf{y})$ in 2.4 reduces to:

$$I(\mathbf{x}; \mathbf{y}) = \log_2 \det(\mathbf{I}_{N_R} + \frac{E_s}{N_T N_0} \mathbf{H} \mathbf{R}_{xx} \mathbf{H}^H) \text{ bps/Hz} \quad (2.8)$$

The capacity of the MIMO channel is given by

$$C = \max \left(\log_2 \det(\mathbf{I}_{N_R} + \frac{E_s}{N_T N_0} \mathbf{H} \mathbf{R}_{xx} \mathbf{H}^H) \right) \text{ bps/Hz} \quad (2.9)$$

Given a bandwidth of B Hz, the maximum achievable data rate over this bandwidth using the MIMO channel is BC bps.

2.1.2 No CSI at the TX

When the TX does not have CSI, the transmitted vector \mathbf{x} is chosen to be statistically non-preferential, i.e. $\mathbf{R}_{xx} = \mathbf{I}_{N_T}$ that implies the signals to be independent and equi-powered at the different TX antennas. The capacity of MIMO channel (2.9) in the absence of CSIT results in the known Shannon capacity:

$$C = \log_2 \det(\mathbf{I}_{N_R} + \frac{E_s}{N_T N_0} \mathbf{H} \mathbf{H}^H) \quad (2.10)$$

Considering the SVD explained in Appendix A, the capacity of the channel can be expressed as:

$$C = \log_2 \det(\mathbf{I}_{N_R} + \frac{E_s}{N_T N_0} \mathbf{U} \mathbf{\Lambda} \mathbf{U}^H) \quad (2.11)$$

using the property of determinants where $\det(\mathbf{I}_N + \mathbf{A} \mathbf{B}) = \det(\mathbf{I}_N + \mathbf{B} \mathbf{A})$ the capacity results to:

$$C = \log_2 \det(\mathbf{I}_{N_R} + \frac{E_s}{N_T N_0} \mathbf{\Lambda}) \quad (2.12)$$

or equivalently:

$$C = \sum_{l=1}^L \log_2(1 + \frac{E_s}{N_T N_0} \lambda_l) \quad (2.13)$$

where L is the rank of the channel and λ_l ($l=1,2,\dots,L$) are the positive eigenvalues of $\mathbf{H} \mathbf{H}^H$. From (2.13), the capacity of the MIMO channel is expressed as the sum of the L SISO channels with power gain λ_l . The optimal power allocation is Uniform Power Allocation (UPA) where each stream gets the same transmitted power $\frac{E_s}{N_T}$.

2.1.3 CSI at the TX

When the TX has information about the channel, the energy at every TX antenna can be adjusted to maximize capacity. Referring to γ_l as the energy allocated at the l -th sub-channel and constraining the total transmitted energy to $\sum_{l=1}^L \gamma_l = N_T$, the mutual information maximization problem now becomes:

$$C = \max_{\sum_{l=1}^L \gamma_l = N_T} \sum_{l=1}^L \log_2(1 + \frac{E_s \gamma_l}{N_T N_0} \lambda_l) \quad (2.14)$$

using the Lagrangian methods, the optimal energy allocation satisfies:

$$\gamma_l^{opt} = (\mu - \frac{N_T N_0}{E_s \lambda_l})_+, l = 1, \dots, L \quad (2.15)$$

constrained to

$$\sum_{l=1}^L \gamma_l^{opt} = N_T \quad (2.16)$$

where μ is a constant and $(x)_+$ implies

$$(x)_+ = \begin{cases} x & \text{if } x \geq 0 \\ 0 & \text{if } x < 0 \end{cases} \quad (2.17)$$

which is the known Water-Filling (WF) algorithm. Figure 2.5 depicts the energy allocation at every sub-channel according to (2.15).

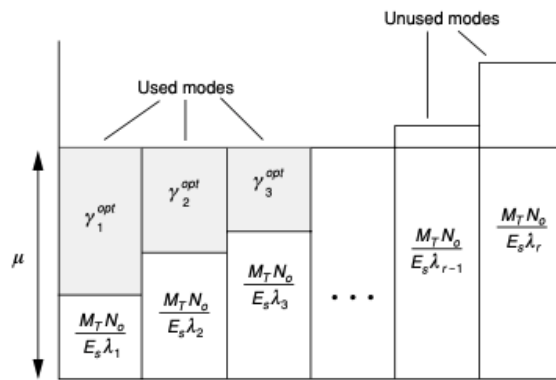


Figure 2.5: Schematic of the power filling algorithm.

Combining the results from this subsection and the previous one, the capacity of a MIMO channel with CSIT can be seen as a sum of L SISO channels, where L is the rank of the channel matrix, with power gain λ_l and the optimal power allocation γ_l from Equation (2.15).

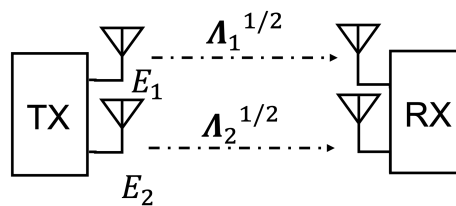


Figure 2.6: P2P Virtual links.

The equivalent channel for a MIMO 2x2 system seen as the sum of independent SISO virtual links can be seen in Figure 2.6. Capacity depends on the TX, so in order to achieve this equivalent channel based on independent links, the TX needs to perform SVD. Figure 2.7 shows a block diagram schematic of the procedure.

Referring \mathbf{h}_{eq} to the equivalent channel that consists of a vector with the eigenvalues of \mathbf{H} , the RX is designed as the matched filter to this equivalent channel, which is: $\frac{\mathbf{h}_{eq}^*}{\|\mathbf{h}_{eq}\|}$.

In practical terms, the precoder of Figure 2.4 is the \mathbf{U}^H matrix and the combiner consists of the \mathbf{V} plus the matched filter.

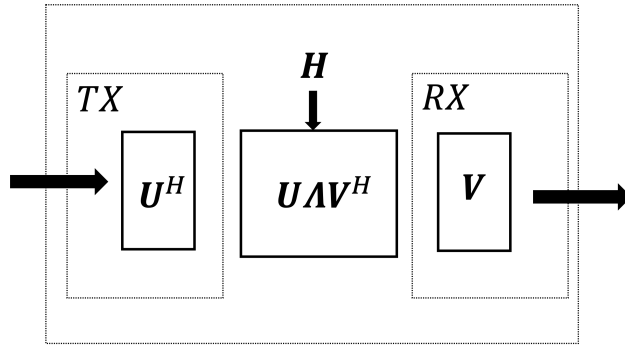


Figure 2.7: Equivalent channel.

2.2 MU-UL with single-antenna UEs

This section describes the system model for the single-antenna UE system scenario. The total number of TX and RX antennas is N_T and N_R , respectively. The $N_R \times 1$ RX signal \mathbf{y} is:

$$\mathbf{y} = \mathbf{W}_R(\mathbf{H}\mathbf{x} + \mathbf{n}) \quad (2.18)$$

where the $N_R \times N_R$ combiner matrix at the RX side is denoted as \mathbf{W}_R , \mathbf{H} is the $N_R \times N_T$ channel matrix, vector \mathbf{x} represents the $N \times 1$ transmitted information and \mathbf{n} the Gaussian Noise vector distributed as $CN \sim (\mathbf{0}_{N_R \times 1}, N_0 \mathbf{I}_{N_R})$.

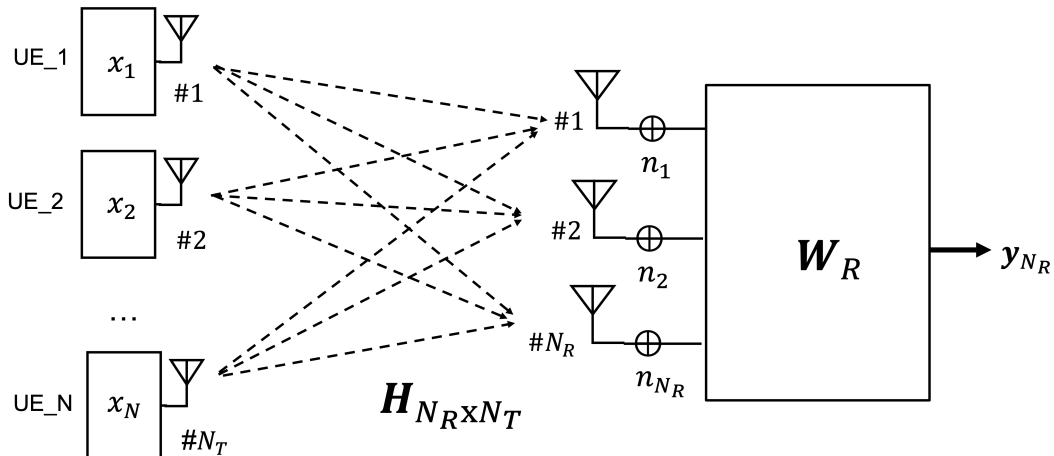


Figure 2.8: System model for MU-UL single-antenna UEs.

2.3 MU-UL with multi-antenna UEs

The system model for the multi-antenna UE scenario is:

$$\mathbf{y} = \mathbf{W}_R(\mathbf{H}\mathbf{W}_T\mathbf{x} + \mathbf{n}) \quad (2.19)$$

where \mathbf{W}_R is the $N_R \times N_R$ combiner matrix, \mathbf{H} the $N_R \times N_T$ channel matrix, \mathbf{W}_T is the $N_T \times N_T$ precoder matrix which is block diagonal and every submatrix in the diagonal is $N_i \times N_i$ where N_i is the number of antennas for the i -th user for a general scenario of N users. \mathbf{x} represents the TX signal vector including the information of the N users and \mathbf{x}_i the information of the i -th user. Vector \mathbf{n} is the AWGN distributed as $CN \sim (\mathbf{0}_{N_R \times 1}, N_0 \mathbf{I}_{N_R})$.

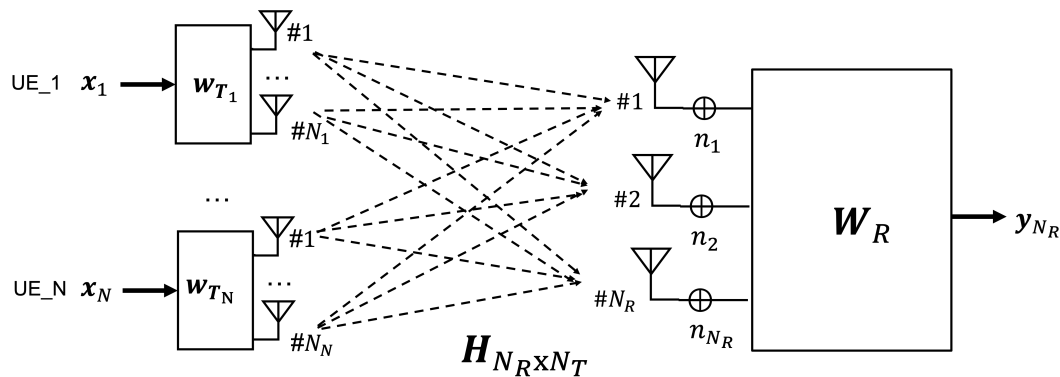


Figure 2.9: System model for MU-UL multi-antenna UEs.

2.4 Architecture design

In the literature, the use of multiple antennas at the RX is often called Space Division Multiple Access (SDMA). The different UEs transmitting at this multi-antenna RX can be differentiated as they produce a different response vector, denoted as signature, at the RX. They are rarely orthogonal between UEs, so the RX needs to do some processing to get the information from every UE correctly. The following content describes the architecture design of the TXs and the RX in a complexity ascending order, first for the single-antenna UEs scenario and, afterward, multi-antenna UEs.

2.4.1 Single-antenna UE

Following the same procedure for the MIMO P2P channel, first the capacity of MU-UL single-antenna UEs will be analyzed in order to motivate the design of the TX that can achieve it. It is remarkable to say that the design of the RX does not depend on capacity, but depending on the RX architecture the capacity region will be achieved or not.

2.4.1.1 Capacity Analysis

Since the UEs in the MU-UL channel are geographically dispersed, they cannot coordinate to transmit to the BS. The data rate that can be reliably maintained simultaneously by all UEs is characterized by a capacity region that will depend on the decoding strategy at the RX - joint decoding or independent decoding [13].

Joint decoding

Joint decoding implies that the signals are detected optimally at the RX via Maximum-Likelihood (ML) detection. If the number of users is N , $\mathbf{R}_{\mathbf{xx}}$ the covariance matrix of the TX signals and \mathbf{H} the channel matrix, the capacity region satisfies:

$$\sum_{k \in N} R_k \leq \log_2 \det(\mathbf{I}_N + \frac{1}{N_0} \mathbf{H} \mathbf{R}_{\mathbf{xx}} \mathbf{H}^H) \text{ bps/Hz} \quad (2.20)$$

where R_k ($k = 1, 2, \dots, N$) is the rate of the k -th user. For example, the capacity region for two users ($N = 2$) satisfies:

$$R_1 \leq \log_2 \left(1 + \frac{E_{s,1}}{N_0} \|\mathbf{h}_1\|^2 \right) \quad (2.21)$$

$$R_2 \leq \log_2 \left(1 + \frac{E_{s,2}}{N_0} \|\mathbf{h}_2\|^2 \right) \quad (2.22)$$

$$R_1 + R_2 \leq \log_2 \det \left(\mathbf{I}_2 + \frac{E_{s,1}}{N_0} \mathbf{h}_1 \mathbf{h}_1^H + \frac{E_{s,2}}{N_0} \mathbf{h}_2 \mathbf{h}_2^H \right) \quad (2.23)$$

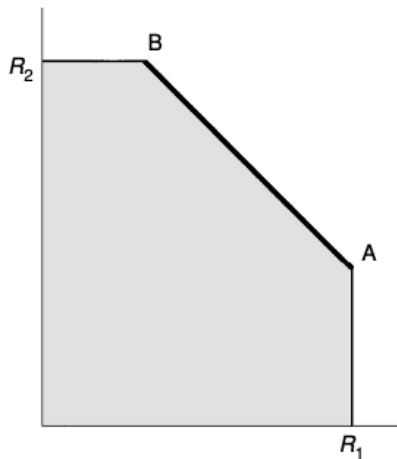


Figure 2.10: MU-UL Capacity region for two UEs.

Figure 2.10 shows the MU-UL channel capacity region for two UEs. At the region's borders, in the vertical line, UE1 transmits at maximum power and treats the signal of UE2 as additional noise. In the horizontal line, UE2 transmits at maximum power and UE1 is treated as noise. All the other points from A to B achieve the maximum sum rate. The capacity region for more than two UEs is polyhedral.

Independent decoding

Independent decoding recovers each user's signal considering all other signals as interfering noise. The RX covariance matrix $\mathbf{R}_{\mathbf{y}\mathbf{y}} = E(\mathbf{y}\mathbf{y}^H)$ is given by

$$\mathbf{R}_{\mathbf{y}\mathbf{y}} = \mathbf{H}\mathbf{R}_{\mathbf{x}\mathbf{x}}\mathbf{H}^H + N_0\mathbf{I}_{N_R} \quad (2.24)$$

The capacity region for independent decoding is the set of all rates that satisfy [14]:

$$R_i \leq \log_2 \left(\frac{\det(\mathbf{R}_{\mathbf{y}\mathbf{y}})}{\det(\mathbf{R}_{\mathbf{y}\mathbf{y}} - E_{s,i} \mathbf{h}_i \mathbf{h}_i^H)} \right), i = 1, 2, \dots, N \quad (2.25)$$

The relationship between the capacity region for independent decoding with respect to joint decoding can be seen in Figure 2.11. Figure 2.12 shows the simplest scenario with two single-antenna UEs and a RX with two antennas.

The overall scenario of this MU-UL system with single-antenna UEs can be seen as a $N_T \times N_R$ MIMO communications channel with N_T TX antennas equal to the number of UEs in the scenario and N_R RX antennas at the BS.

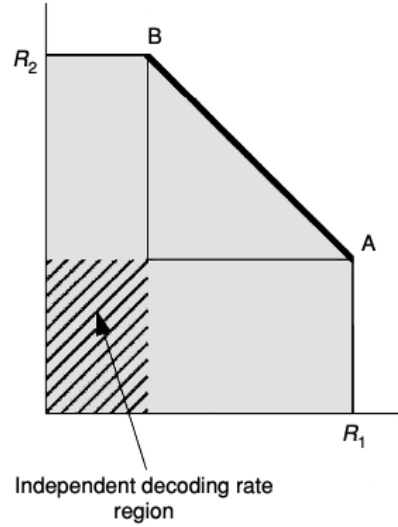


Figure 2.11: MU-UL Capacity region for two UEs with independent decoding at the RX.

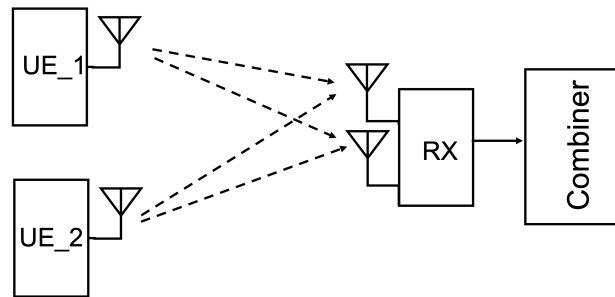


Figure 2.12: MU-UL single-antenna UEs.

In a typical MIMO system such as the one studied in Section 2.1, the design of the TX that achieved capacity was the SVD. The main difference with the scenario in the previous section is that the UEs of the MU-UL have information about its individual channel but not from other UEs, therefore the channel cannot be diagonalized.

For that reason, instead of channel diagonalization, the combiner at the BS consists of a beamformer that cancels or attenuates the interference that every user produces to others. Depending on the beamformer used (RX architecture), the system will be able to achieve capacity or not.

In this thesis, three common beamformers will be studied: Zero Forcing (ZF), QR and Minimum Mean Squared Error (MMSE). The first one completely nulls the interference from other users, the MMSE attenuates its effect and QR performance is in between the ZF and MMSE.

2.4.1.2 ZF Beamformer

The ZF beamformer is designed such that the output signal at every RX antenna contains only information about a specific UE, whereas other UEs are canceled. The beamformer \mathbf{W}_R^H is steered to the appropriate UE channel vector and orthogonal to others. In practice, the multiplication of $\mathbf{W}_R^H \mathbf{H}$ results in a diagonal matrix.

$$\mathbf{W}_R^H \mathbf{H} = \begin{pmatrix} \mathbf{w}_{R1}^H \\ \mathbf{w}_{R2}^H \end{pmatrix} (\mathbf{h}_1 \quad \mathbf{h}_2) = \begin{pmatrix} \alpha_1 & 0 \\ 0 & \alpha_2 \end{pmatrix} \quad (2.26)$$

The beamformers are:

$$\mathbf{w}_{R1} = \left(\mathbf{I} - \frac{\mathbf{h}_2 \mathbf{h}_2^H}{|\mathbf{h}_2|^2} \mathbf{h}_1 \frac{1}{z_1} \right); \mathbf{w}_{R2} = \left(\mathbf{I} - \frac{\mathbf{h}_1 \mathbf{h}_1^H}{|\mathbf{h}_1|^2} \mathbf{h}_2 \frac{1}{z_2} \right) \quad (2.27)$$

z_1 and z_2 are constants to make the vectors unitary.

Spatial explanation

The ZF is also known as interference nulling or decorrelator [15] and can be understood as the combination of the projection operation followed by a matched filter. Since the projection and matched filtering are linear operations, the ZF is also a linear filter.

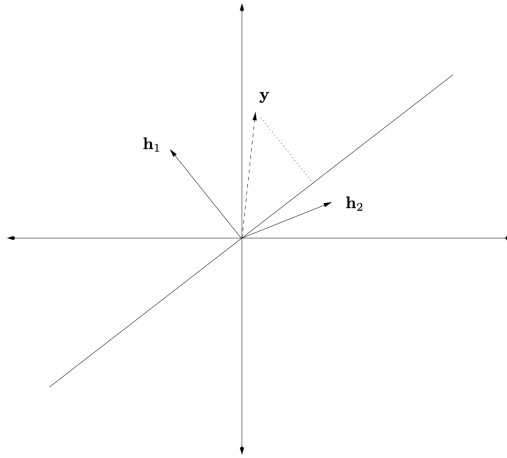


Figure 2.13: Schematic representation of the projection operation.

The ZF projects the RX \mathbf{y} signal onto the subspace orthogonal to the one spanned by the channel vectors from other UEs. A geometric description of the projection operation of vector \mathbf{y} onto the subspace orthogonal to \mathbf{h}_1 is in Figure 2.13.

The RX signal is:

$$\mathbf{y} = \mathbf{W}_R^H (\mathbf{H}\mathbf{x} + \mathbf{n}) = \begin{pmatrix} \alpha_1 & 0 \\ 0 & \alpha_2 \end{pmatrix} \begin{pmatrix} x_1 \\ x_2 \end{pmatrix} + \begin{pmatrix} \tilde{n}_1 \\ \tilde{n}_2 \end{pmatrix}$$

The rate for every UE is $r_i = \log_2(1 + \alpha_i^2 E_i)$.

2.4.1.3 QR Beamformer

The idea of the QR beamformer is that the first UE allows interference from other UEs and the following UEs are orthogonal to previous UEs, i.e., UE2 is orthogonal to UE1, UE3 is orthogonal to UE1 and UE2...

In other words, for the first UE the beamformer is steered to its channel vector and for the second UE the beamformer is orthogonal to the previous UE and steered to himself:

$$\mathbf{w}_{R_1} = \frac{\mathbf{h}_1}{|\mathbf{h}_1|}; \mathbf{w}_{R_2} = \left(\mathbf{I} - \frac{\mathbf{h}_1 \mathbf{h}_1^H}{|\mathbf{h}_1|^2} \mathbf{h}_2 \frac{1}{z_2} \right)$$

The RX starts by decoding the UE without interference (the one with the highest index) to avoid error propagation. With the procedure of the known Signal Interference Canceller (SIC), it removes the contribution that this UE produces to others by multiplying the already decoded symbol with the equivalent channel coefficient that resulted from the diagonal of $\mathbf{H}_{eq} = \mathbf{W}_R^H \mathbf{H}$. After the subtraction the information of the UE can be decoded. Figure 2.14 depicts the SIC for three UEs. $\mathbf{y}_1, \mathbf{y}_2$ and \mathbf{y}_3 refer to the RX signal at the RX antenna 1, 2 and 3 respectively after applying the beamformer matrix. Symbols \hat{x}_1, \hat{x}_2 and \hat{x}_3 are the decoded symbols.

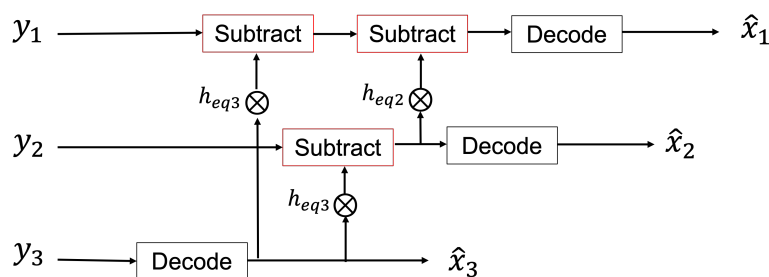


Figure 2.14: SIC for three UEs.

The name of this beamformer is due to the QR decomposition of the channel ([16]). $QR(\mathbf{H}) = \mathbf{Q}\mathbf{R}$ where \mathbf{Q} is an orthogonal matrix ($\mathbf{Q}\mathbf{Q}^H = \mathbf{I}$) and \mathbf{R} is upper triangular. The RX beamformer is $\mathbf{W}_R^H = \mathbf{Q}^H$, at the RX side $\mathbf{W}_R^H \mathbf{H} = \mathbf{Q}^H \mathbf{Q}\mathbf{R} = \mathbf{R} = \begin{pmatrix} r_{11} & r_{12} \\ 0 & r_{22} \end{pmatrix}$.

The RX signal is:

$$\mathbf{y} = \mathbf{W}_R^H (\mathbf{H}\mathbf{x} + \mathbf{n}) = \begin{pmatrix} |\mathbf{h}_1| & r_{12} \\ 0 & \alpha_2 \end{pmatrix} \begin{pmatrix} x_1 \\ x_2 \end{pmatrix} + \begin{pmatrix} \tilde{n}_1 \\ \tilde{n}_2 \end{pmatrix}$$

First, the RX decodes the information of UE2 (x_2), then with SIC removes the interference that UE2 produces to UE1, and finally, the information of UE1 (x_1) is decoded. The rate for the first UE is the maximum $r_1 = \log_2(1 + |\mathbf{h}_1|^2 E_1)$ and for UE2 it depends on the constant α_2 , $r_2 = \log_2(1 + |\alpha_2|^2 E_2)$.

2.4.1.4 MMSE

From the last subsection, the QR Beamformer tolerates interference from new UEs but not for the previous ones. The MMSE Beamformer, instead of nulling the previous UEs they are mitigated with the MMSE. The first UE is matched to its channel vector and the second is steered to \mathbf{h}_2 and attenuates \mathbf{h}_1 by MMSE.

The beamformers are

$$\mathbf{w}_{R_1} = \frac{\mathbf{h}_1}{|\mathbf{h}_1|}; \mathbf{w}_{R_2} = (\mathbf{I} + E_1 \mathbf{h}_1 \mathbf{h}_1^H)^{-1} \frac{\mathbf{h}_2}{|z_2|}$$

$$\text{For } N \text{ UEs: } \mathbf{w}_{R_n} = \left(\mathbf{I} + \sum_{i=1}^{n-1} E_i \mathbf{h}_i \mathbf{h}_i^H \right)^{-1} \frac{\mathbf{h}_{R_n}}{z_{R_n}} \quad (2.28)$$

The RX signal is:

$$\mathbf{y} = \mathbf{W}_R^H (\mathbf{H}\mathbf{x} + \mathbf{n}) = \begin{pmatrix} |\mathbf{h}_1| & r_{12} \\ \epsilon_2 & \alpha_2 \end{pmatrix} \begin{pmatrix} x_1 \\ x_2 \end{pmatrix} + \begin{pmatrix} \tilde{n}_1 \\ \tilde{n}_2 \end{pmatrix}$$

First, the RX decodes the information from UE2 (x_2) with interference from UE1, then with SIC the interference of UE2 is removed from UE1 and (x_1) can be decoded. The UEs should be ordered considering its channel conditions: from the worst to the best. The UE decoded with interference should have the best channel conditions to avoid error propagation to others.

The rate of UE1 after implementing SIC is $r_1 = \log_2(1 + |\mathbf{h}_1|^2 E_1)$ and the rate of UE2 is $r_2 = \log_2(1 + |\epsilon_2|^2 E_1 + |\alpha_2|^2 E_2)$. The block diagram scheme of the SIC after applying the MMSE beamformers is the same as for the QR in Figure 2.14. The difference is that the input symbols y_1 to y_3 will be acquired with the MMSE beamformers instead of the QR.

2.4.1.5 From ZF to MMSE

As explained in Section 2.4.1.2, the ZF nulled the interference produced by other UEs, no matter how much energy of the stream of interest is lost. This RX strategy performs well in a high SNR regime as the interference from other UEs is very high and is dominant over the Gaussian noise. On the contrary, in a low SNR regime, the interference is not that high and matched filtering or the maximal ratio combining (MRC) is a better strategy.

Imagining a SIMO system such as the one in Figure 2.2, the MRC weights the RX signal in each branch in proportion to the signal strength and also aligns the phases of the signals in the summation to maximize the output SNR. If the channel vector is \mathbf{h} , the MRC is $\frac{\mathbf{h}^H}{\|\mathbf{h}\|}$.

The motivation is to find a linear RX that optimally deals with the interference and background noise that maximizes the signal-to-interference plus noise ratio (SINR) for any value of the SNR acting like the ZF for high SNR and the Matched Filter at low SNR. The problem can be thought of as the generalization of the RX beamforming to the case when there is interference and noise. Following the explanation from [15], the derivation of the MMSE RX will be done by looking at a general channel vector formulation:

$$\mathbf{y} = \mathbf{h}x + \mathbf{z} \quad (2.29)$$

x is the TX symbol that needs to be estimated. \mathbf{h} is the deterministic channel vector with a length equal to the number of RX antennas (N_R) and \mathbf{y} is the RX vector. \mathbf{z} is complex circular symmetric colored noise which contains the noise plus the interference from other UEs and with an invertible covariance matrix \mathbf{K} . \mathbf{z} and x are assumed to be uncorrelated.

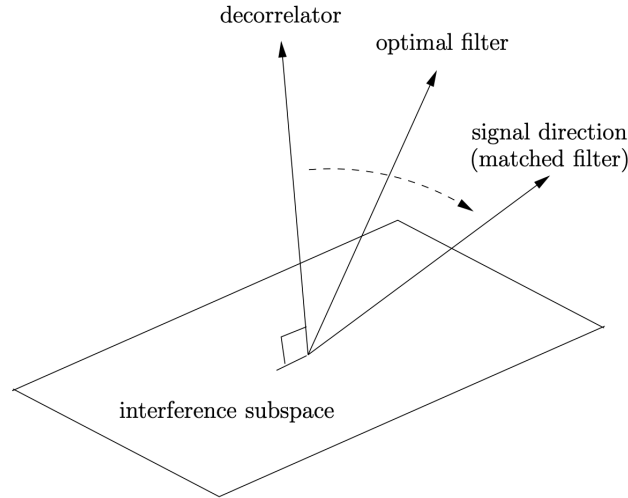


Figure 2.15: Optimal filter that goes from ZF at high SNR to the Matched Filter at low SNR.

If the noise is white, then the optimal RX is to project \mathbf{y} onto the direction along \mathbf{h} . As \mathbf{z} is colored, a whitening noise step is needed before. First, \mathbf{y} is passed through the invertible linear transformation $\mathbf{K}^{-\frac{1}{2}}$ such that the noise becomes white ($\tilde{\mathbf{z}}$):

$$\mathbf{K}^{-\frac{1}{2}}\mathbf{y} = \mathbf{K}^{-\frac{1}{2}}\mathbf{h}x + \tilde{\mathbf{z}} \quad (2.30)$$

Matrix \mathbf{K} is an invertible covariance matrix that can be written as $\mathbf{U}\mathbf{\Lambda}\mathbf{U}^*$, where \mathbf{U} is a rotation matrix and diagonal matrix $\mathbf{\Lambda}$ has positive diagonal elements. $\mathbf{K}^{\frac{1}{2}}$ is defined as the $\mathbf{U}\mathbf{\Lambda}^{\frac{1}{2}}\mathbf{U}^*$ where $\mathbf{\Lambda}^{\frac{1}{2}}$ is a diagonal matrix with elements equal to the square root of the diagonal elements in $\mathbf{\Lambda}$.

Afterward the output in (2.30) is projected in the direction of $\mathbf{K}^{-\frac{1}{2}}\mathbf{h}$ to get an effective scalar channel:

$$\left(\mathbf{K}^{-\frac{1}{2}}\mathbf{h}\right)^* \mathbf{K}^{-\frac{1}{2}}\mathbf{y} = \mathbf{h}^*\mathbf{K}^{-1}\mathbf{y} = \mathbf{h}^*\mathbf{K}^{-1}\mathbf{h}x + \mathbf{h}^*\mathbf{K}^{-1}\mathbf{z} \quad (2.31)$$

The linear RX that maximizes the SNR is

$$\mathbf{v}_{MMSE} := \mathbf{K}^{-1}\mathbf{h} \quad (2.32)$$

In [15], it is shown that this RX, with appropriate scaling, minimizes the MSE in estimating x , that gives the MMSE name to the RX. Further development can be found in Appendix C. The SINR achieved is:

$$\sigma_x^2 \mathbf{h}^* \mathbf{K}^{-1} \mathbf{h} \quad (2.33)$$

The RX stream of the k -th UE can be written as

$$\mathbf{y}[m] = \mathbf{h}_k x_k[m] + \mathbf{z}_k[m] \quad (2.34)$$

where x_k is the TX symbol, \mathbf{h}_k the channel vector of the UE with length the number of RX antennas, \mathbf{z}_k is the noise plus interference faced by stream k and \mathbf{n} is purely noise:

$$\mathbf{z}_k[m] = \sum_{i \neq k} \mathbf{h}_i x_i[m] + \mathbf{n}[m] \quad (2.35)$$

The invertible covariance matrix \mathbf{K} of \mathbf{z} is:

$$\mathbf{K} = N_0 \mathbf{I}_{N_R} + \sum_{i \neq k}^{N_T} E_i \mathbf{h}_i \mathbf{h}_i^* \quad (2.36)$$

where E_i is the energy associated to the i -th stream. Substituting this expression to equations (2.32) and (2.33) the linear RX for the k -th stream is:

$$\left(N_0 \mathbf{I}_{N_R} + \sum_{i \neq k}^{N_T} E_i \mathbf{h}_i \mathbf{h}_i^* \right)^{-1} \mathbf{h}_k \quad (2.37)$$

and SINR

$$E_k \mathbf{h}_k^* \left(N_0 \mathbf{I}_{N_R} + \sum_{i \neq k}^{N_T} E_i \mathbf{h}_i \mathbf{h}_i^* \right)^{-1} \mathbf{h}_k \quad (2.38)$$

Performance

The motivation to design such an optimal linear MMSE RX was to find a RX that acted between a decorrelator (ZF) at high SNR and a matched filtering at low SNR. Analyzing the covariance matrix in Equation (2.36), at a low SNR regime, the interference from other UEs is very low compared to N_0 , so the covariance matrix can be approximated as

$$\mathbf{K} \approx N_0 \mathbf{I}_{N_R} \quad (2.39)$$

and the MMSE RX in (2.37) reduces to the matched filter. On the other hand, at a high SNR regime the \mathbf{K}^{-1} operation reduces to the projection of \mathbf{y} onto the subspace orthogonal to the one spanned by the different channel vectors $\mathbf{h}_1, \dots, \mathbf{h}_{k-1}, \mathbf{h}_{k+1}, \dots, \mathbf{h}_{N_T}$ and the linear MMSE RX reduces to the ZF.

Capacity analysis

From the MMSE RX derived in this subsection, without SIC the maximum rate that the k -th stream can reliably carry is

$$C_k = \log_2 \left(1 + E_k \mathbf{h}_k^* \mathbf{K}_k^{-1} \mathbf{h}_k \right) \quad (2.40)$$

Figure 2.16 from [15] plots the performance in terms of the ratio between rate and capacity

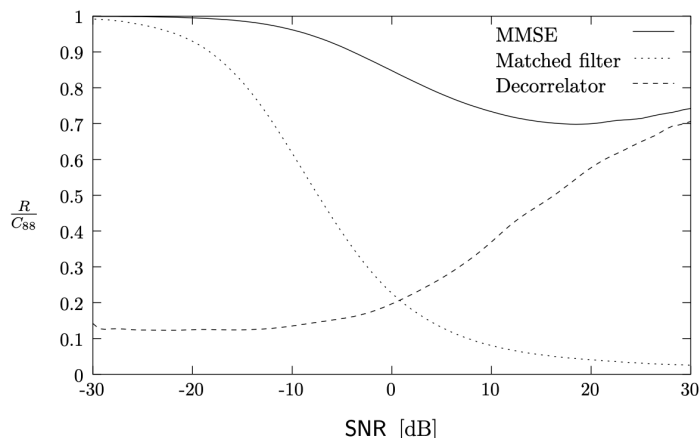


Figure 2.16: Comparison of the rate-capacity ratio of different RXs.

for the different RXs: MMSE, Matched Filter and the decorrelator (ZF) with equal power allocation over an i.i.d. Rayleigh fading channel. It can be seen that the MMSE filter

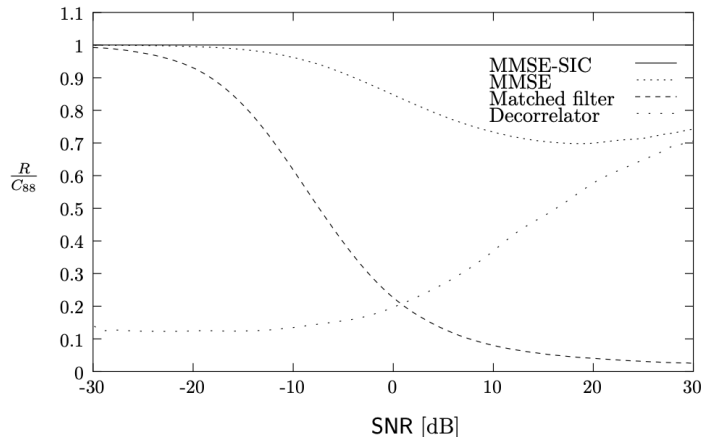


Figure 2.17: MMSE-SIC achieves capacity for an i.i.d. Rayleigh fading channel.

performs better than the others for the entire SNR range.

If the MMSE filter is upgraded with an additional SIC block, the performance is clearly improved and the MMSE-SIC is optimal such that it achieves the maximum possible sum rate, see Figure 2.17. Referring as $SINR_k$ the $SINR$ of the k -th UE and the corresponding rate to $\log_2(1 + SINR_k)$, the rates sum up to

$$\sum_{k=1}^K \log_2(1 + SINR_k) = \log_2 \det \left(\mathbf{I}_{N_R} + \frac{1}{N_0} \mathbf{H} \mathbf{R}_{xx} \mathbf{H}^* \right) \quad (2.41)$$

which is the best possible sum rate.

MMSE filter achieves capacity as it is information lossless. The linear MMSE RX ($\mathbf{v}_{MMSE} = \mathbf{K}^{-1} \mathbf{h}$) not only maximizes the SNR but also provides a sufficient statistics to detect \mathbf{x} , which means that is information lossless:

$$I(x; \mathbf{y}) = I(x; \mathbf{v}_{mmse}^* \mathbf{y}) \quad (2.42)$$

The justification is further developed in Appendix D.

However, the summation from expression (2.37) considers all the UEs, but in (2.28) only prior UEs are taken into account. The following content explains why only prior UEs are relevant.

According to [15], if the RX signal is

$$\mathbf{y} = \mathbf{H} \mathbf{x} + \mathbf{n} \quad (2.43)$$

and the input is $\mathcal{CN} \sim (\mathbf{0}, \text{diag}(E_1, \dots, E_{N_T}))$, the mutual information between \mathbf{x} and \mathbf{y} is

$$\begin{aligned} I(\mathbf{x}; \mathbf{y}) &= I(x_1, x_2, \dots, x_{N_T}; \mathbf{y}) \\ &= I(x_1; \mathbf{y}) + I(x_2; \mathbf{y} | x_1) + \dots + I(x_{N_T}; \mathbf{y} | x_1, \dots, x_{N_T-1}) \end{aligned} \quad (2.44)$$

that is consequence of the chain rule of mutual information. Looking at the k -th term in the chain rule expression: $I(x_k; \mathbf{y} | x_1, \dots, x_{k-1})$, conditioning means that the information is known so this terms can be subtracted from the output:

$$\mathbf{y}' = \mathbf{y} - \sum_{i=1}^{k-1} \mathbf{h}_i x_i = \mathbf{h}_k x_k + \sum_{i>k} \mathbf{h}_i x_i + \mathbf{n} \quad (2.45)$$

Thus $I(x_k; \mathbf{y} | x_1, \dots, x_{k-1}) = I(x_k; \mathbf{y}') = I(x_k; \mathbf{v}_{MMSE}^* \mathbf{y}')$. The interference terms that must be attenuated in the beamformers for the k -th UE in (2.37) are only those produced by the UEs whose index is higher than k . Our system, considers that the UEs are ordered from the weakest ($k = 1$) to the strongest ($k = N$). That is the reason why in (2.28) the interference of previous UEs ($i < k$) is subtracted instead of posterior UEs ($i > k$).

2.4.2 Multi-antenna UEs

The scenario becomes more complex when UEs have more than one antenna. Depending on the UE's interest, the spatial diversity that multiple antennas introduce can be used to send different or the same information to the RX. As it was pointed out at the beginning of this thesis, it will be assumed that different information is sent to every antenna.

The following Figure 2.18 depicts the scenario of two UEs with two antennas and a RX with 4 antennas. If every TX antenna sends different bits of information, in order to properly decode every stream the total number of antennas at the RX must be higher or equal to the total number of TX antennas.

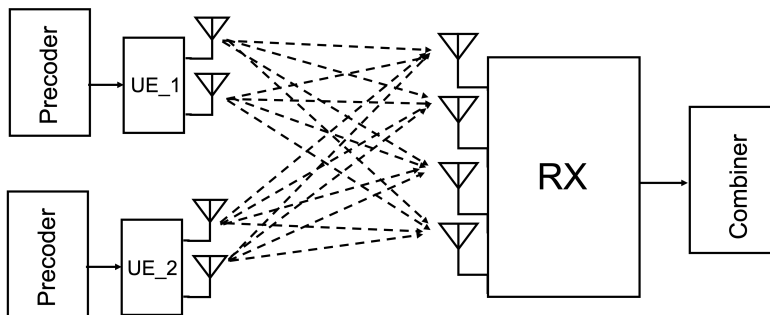


Figure 2.18: MU-UL multi-antenna UEs.

2.4.2.1 Capacity Analysis

The optimal power allocation for this MU-UL with multi-antenna UEs is the WF algorithm for every UE subchannel matrix, similar to the procedure for the MIMO P2P scenario. The capacity region is depicted in Figure 2.19.

The following subsection describes the architecture of the TX which has been designed in order to attain capacity. Afterward, the different RX beamformers are presented and similar to the single-antenna scenario, the RX MMSE has been proven to achieve capacity.

2.4.2.2 TX side

Every TX has to design its own precoder based on the vectors from the channel matrix that affect their antennas. As it was mentioned in Section 2.4, every TX has CSI knowledge of its channel vector, but not from others.

Consequently, to achieve capacity each TX has to diagonalize its subchannel matrix and allocate the power according to the WF computed with the eigenvalues of this UE subchannel SVD. Additionally, every UE generates their \mathbf{U}_{iMU-UL} matrix that contains the

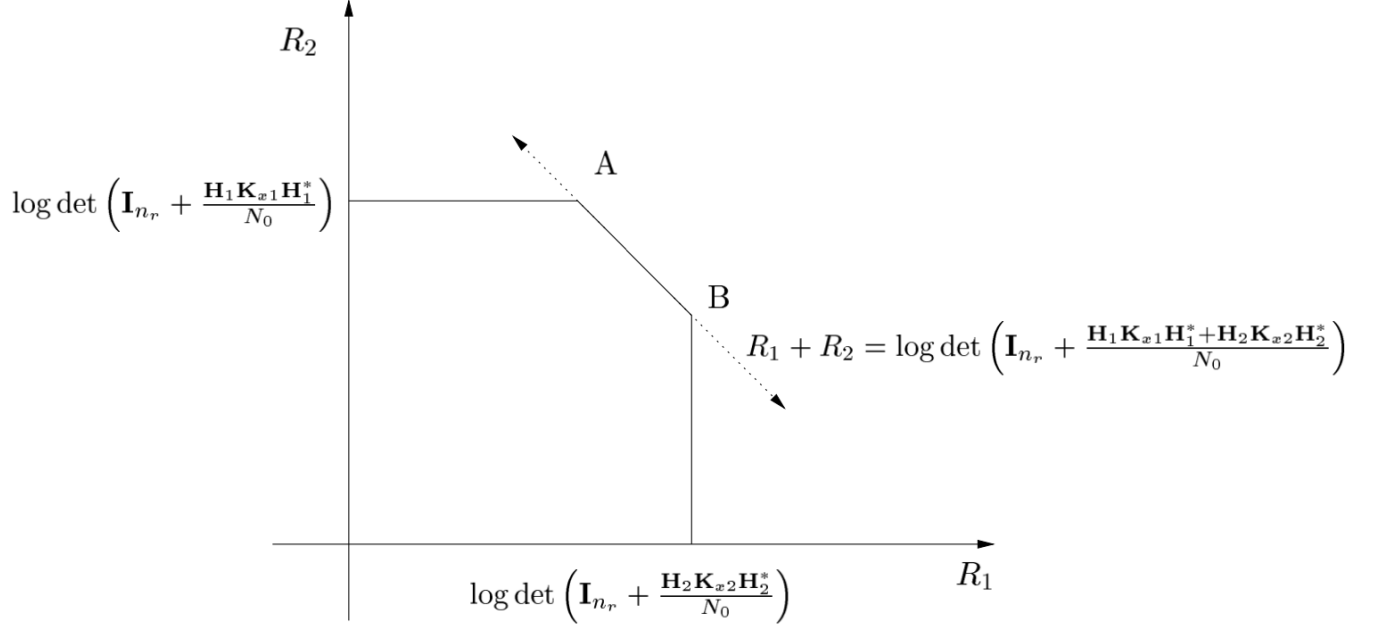


Figure 2.19: Capacity region for two multi-antennas UEs.

left eigenvectors of their subchannel.

For the previously mentioned scenario the channel matrix is:

$$\mathbf{H}_{44} = \begin{pmatrix} \mathbf{h}_1 & \mathbf{h}_2 & \mathbf{h}_3 & \mathbf{h}_4 \end{pmatrix} = \begin{pmatrix} h_{11} & h_{12} & h_{13} & h_{14} \\ h_{21} & h_{22} & h_{23} & h_{24} \\ h_{31} & h_{32} & h_{33} & h_{34} \\ h_{41} & h_{42} & h_{43} & h_{44} \end{pmatrix} \quad (2.46)$$

where \mathbf{h}_1 and \mathbf{h}_2 refers to the first UE (first and second antenna respectively) meanwhile, \mathbf{h}_3 and \mathbf{h}_4 to the second UE. Each TX performs SVD with its 2×2 subchannel and the right eigenvectors generate the \mathbf{U}_i $MU-UL$ 2×2 .

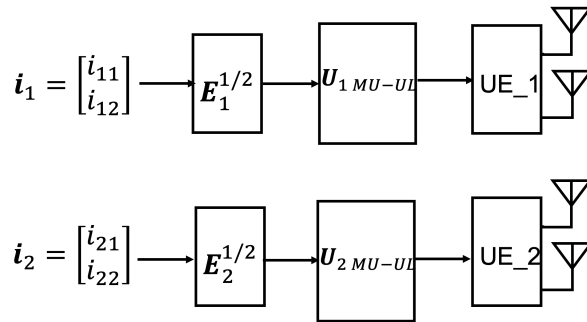


Figure 2.20: TX block MU-UL channel with multiple antennas.

Every \mathbf{U}_i $MU-UL$ matrix results from the SVD of the i -th UE channel matrix:

$$\mathbf{H}_i = \mathbf{V}_i \mathbf{\Lambda}_i \mathbf{U}_i^H \quad (2.47)$$

In Figure 2.20 vectors \mathbf{i} represent the symbols generated with energy equal to 1, then the

diagonal matrix $\mathbf{E}_i^{1/2}$ gives the necessary energy to each symbol. The resulting vector $\mathbf{x} = \mathbf{i}\mathbf{E}_i^{1/2}$ is the \mathbf{x} vector from the system model in Section 2.3.

The final signal TX to the channel is:

$$\begin{aligned} \mathbf{s}_1 &= \mathbf{U}_1 \mathbf{U}_{MU-UL} \mathbf{E}_1^{1/2} \mathbf{i}_1 = \mathbf{U}_{MU-UL 2 \times 2} \begin{pmatrix} E_{11}^{1/2} & 0 \\ 0 & E_{22}^{1/2} \end{pmatrix} \begin{pmatrix} i_{11} \\ i_{12} \end{pmatrix} \\ \mathbf{s}_2 &= \mathbf{U}_2 \mathbf{U}_{MU-UL} \mathbf{E}_2^{1/2} \mathbf{i}_2 = \mathbf{U}_{MU-UL 2 \times 2} \begin{pmatrix} E_{33}^{1/2} & 0 \\ 0 & E_{44}^{1/2} \end{pmatrix} \begin{pmatrix} i_{21} \\ i_{22} \end{pmatrix} \end{aligned}$$

They can be arranged in a single form considering \mathbf{U}_{MU-UL} a block diagonal matrix:

$$\mathbf{s}_T = \begin{pmatrix} \mathbf{s}_1 \\ \mathbf{s}_2 \end{pmatrix} = \mathbf{U}_{MU-UL} \mathbf{E}^{1/2} \mathbf{i} = \begin{pmatrix} \mathbf{U}_1 \mathbf{U}_{MU-UL} & \mathbf{0}_{2 \times 2} \\ \mathbf{0}_{2 \times 2} & \mathbf{U}_2 \mathbf{U}_{MU-UL} \end{pmatrix} \begin{pmatrix} \mathbf{E}_1^{1/2} & \mathbf{0}_{2 \times 2} \\ \mathbf{0}_{2 \times 2} & \mathbf{E}_2^{1/2} \end{pmatrix} \begin{pmatrix} \mathbf{i}_1 \\ \mathbf{i}_2 \end{pmatrix}$$

2.4.2.3 RX side

To complete the subchannel SVD on the RX side, the first step is multiplying by matrix \mathbf{V} that contains the left eigenvectors of the SVD of \mathbf{H} . \mathbf{H}_{eq} matrix is used to refer to this SVD of the channel with the block diagonal matrix \mathbf{U}_{MU-UL} and \mathbf{V} . The resulting \mathbf{A}_i sub-matrices have 2x2 dimensions:

$$\mathbf{H}_{eq} = \mathbf{V}^H \mathbf{H} \mathbf{U}_{MU-UL} = \begin{pmatrix} \mathbf{A}_1 & \mathbf{A}_2 \\ \mathbf{A}_3 & \mathbf{A}_4 \end{pmatrix} \quad (2.48)$$

The second step on the RX side is designing the beamformers (ZF, QR or MSE) so that the UEs interference is canceled or attenuated.

ZF Beamformer

The ZF beamformer is designed such that the resulting matrix $\mathbf{B}_{ZF}^H \mathbf{H}_{eq}$ is block diagonal. Now instead of orthogonal vectors (single-antenna case), orthogonal matrices are needed for multi-antenna UEs. The beamformer corresponding to UE1 (\mathbf{B}_1) has to be orthogonal to the \mathbf{A}_2 matrix (from UE2) to avoid interference. The vice-versa applies with the beamformer of UE2 (\mathbf{B}_2) with respect to UE1 (\mathbf{A}_3).

$$\mathbf{B}_{ZF}^H \mathbf{H}_{eq} = \begin{pmatrix} \mathbf{B}_1^H \\ \mathbf{B}_2^H \end{pmatrix} \begin{pmatrix} \mathbf{A}_1 & \mathbf{A}_2 \\ \mathbf{A}_3 & \mathbf{A}_4 \end{pmatrix} = \begin{pmatrix} \mathbf{C}_1 & \mathbf{0} \\ \mathbf{0} & \mathbf{C}_2 \end{pmatrix}$$

The beamformer matrix for every UE is computed in the same way as in equation (2.27) but substituting matrices for vectors.

QR Beamformer

When it comes to the QR beamformer, the idea is the same as for single-antenna UEs. The beamformer for UE1 is steered to his channel matrix leaving some interference denoted as \mathbf{Int} . For UE2 the beamformer is orthogonal to the channel matrix of UE1.

$$\mathbf{B}_{QR}^H \mathbf{H}_{eq} = \begin{pmatrix} \mathbf{B}_1^H \\ \mathbf{B}_2^H \end{pmatrix} \begin{pmatrix} \mathbf{A}_1 & \mathbf{A}_2 \\ \mathbf{A}_3 & \mathbf{A}_4 \end{pmatrix} = \begin{pmatrix} \mathbf{C}_1 & \mathbf{Int} \\ \mathbf{0} & \mathbf{C}_2 \end{pmatrix} \quad (2.49)$$

MMSE Beamformer

The MMSE beamformer for UE1 is steered to its channel matrix leaving some interference from other UEs. For UE2 the MMSE RX mitigates the interference from UE1 and suffers from residual interference denoted as ε .

$$\mathbf{B}_{MSE}^H \mathbf{H}_{eq} = \begin{pmatrix} \mathbf{B}_1^H \\ \mathbf{B}_2^H \end{pmatrix} \begin{pmatrix} \mathbf{A}_1 & \mathbf{A}_2 \\ \mathbf{A}_3 & \mathbf{A}_4 \end{pmatrix} = \begin{pmatrix} \mathbf{C}_1 & \mathbf{Int} \\ \varepsilon & \mathbf{C}_2 \end{pmatrix} \quad (2.50)$$

2.4.2.4 Final SVD decomposition

The third step is performing SVD again for every UE with their submatrices so that the interference between antennas from the same UE is deleted.

For the simplest scenario, after the ZF beamformer the matrix results in the following:

$$\begin{pmatrix} \mathbf{C}_1 & \mathbf{0} \\ \mathbf{0} & \mathbf{C}_2 \end{pmatrix};$$

Every UE computes the SVD of his subchannel:

$$\mathbf{C}_1 = \begin{pmatrix} c_{11} & c_{12} \\ c_{21} & c_{22} \end{pmatrix} = \mathbf{V}_{C1} \mathbf{\Lambda}_{C1}^{1/2} \mathbf{U}_{C1}^H$$

$$\mathbf{C}_2 = \begin{pmatrix} c_{33} & c_{34} \\ c_{43} & c_{44} \end{pmatrix} = \mathbf{V}_{C2} \mathbf{\Lambda}_{C2}^{1/2} \mathbf{U}_{C2}^H$$

The left eigenvector matrix that has to be applied at the RX side is:

$$\mathbf{V}_C^H = \begin{pmatrix} \mathbf{V}_{C1}^H & \mathbf{V}_{C2}^H \end{pmatrix}$$

and each i -th UE needs to include matrix \mathbf{U}_{C_i} at the TX.

After all the procedures, there is no interference from one UE to another for the ZF beamformer as the final matrix between the TX and the RX is:

$$\begin{pmatrix} d_{11} & 0 & 0 & 0 \\ 0 & d_{22} & 0 & 0 \\ 0 & 0 & d_{33} & 0 \\ 0 & 0 & 0 & d_{44} \end{pmatrix}$$

On the contrary, the QR and MSE beamformers allow interference from previous UEs so a SIC block is needed at the end of the RX side. After the final SVD decomposition and the SIC block, the matrix between the TX and the RX for the QR will be diagonal but for the MMSE it will have some residual coefficients shown in (2.51).

$$\begin{pmatrix} d_{11} & 0 & 0 & 0 \\ 0 & d_{22} & 0 & 0 \\ \epsilon_{31} & \epsilon_{32} & d_{33} & 0 \\ \epsilon_{41} & \epsilon_{42} & 0 & d_{44} \end{pmatrix} \quad (2.51)$$

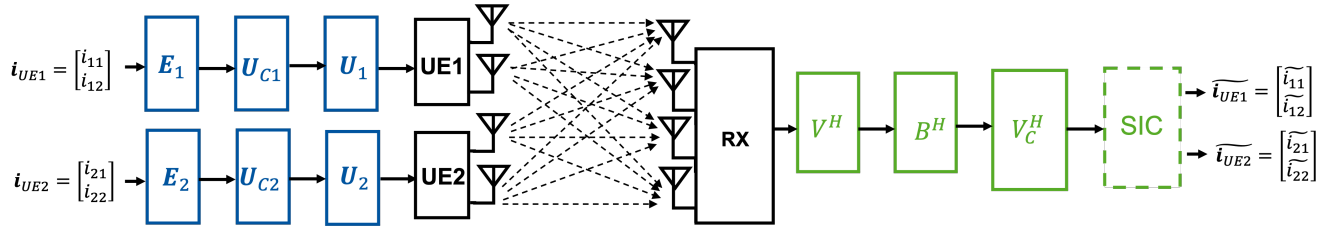


Figure 2.21: Complete TX and RX chain.

Figure 2.21 depicts the final block diagram for two UEs with the SIC block, the final SVD decomposition in matrices \mathbf{U}_C , \mathbf{V}_C , the beamformers \mathbf{B} and the SVD of the individual UEs channel matrices due to WF in \mathbf{U} and \mathbf{V} . According to the system model in Section 2.3, the precoder \mathbf{W}_T for the i -th UE is $\mathbf{W}_{T,i} = \mathbf{U}_i \mathbf{U}_{C,i} \mathbf{E}_i \mathbf{i}_{UEi}$. The combiner matrix at the RX part is $\mathbf{W}_R^H = \mathbf{V}_C^H \mathbf{B}^H \mathbf{V}^H$.

3 Performance analysis

The software simulator of MU-UL was implemented in C programming language. The main library used in the project is GNU Scientific Library (GSL) providing implementation of linear algebra operation over vectors and matrices. A difficulty with this GSL library is the lack of SVD functions for complex-valued matrices; only the Eigenvector Decomposition (EVD) is possible. In order to do complex SVD, the relationship between EVD to SVD explained in Appendix A was exploited. The analysis of results and figures plotting was done with Python.

3.1 Simulator implementation

The following Subsections provide a pseudocode and a flow chart of the SW implemented.

3.1.1 Pseudocode

```

for SNR levels do
  for iterations do
    Generate channel matrix  $\mathbf{H}$ 
    Channel SVD
    if users>1 AND multi-antenna-users then
      SVD of each user subchannel
    end if
    if users>1 then
      Generate beamformers
    end if
    if users>1 AND multi-antenna-users then
      Final SVD
    end if
    Order channel according to eigenvalues
    Power allocation
    Generate precoder and combiner ( $\mathbf{W}_T$ ,  $\mathbf{W}_R$ )
    Generate symbols
    Apply precoder ( $\mathbf{W}_T$ )
    Go to channel + noise
    Apply combiner ( $\mathbf{W}_R$ )
    SIC
    Remove channel
    Decode symbols
    Compute BER
    Compute rates and capacity
  end for
end for

```


3.1.2 Flow chart

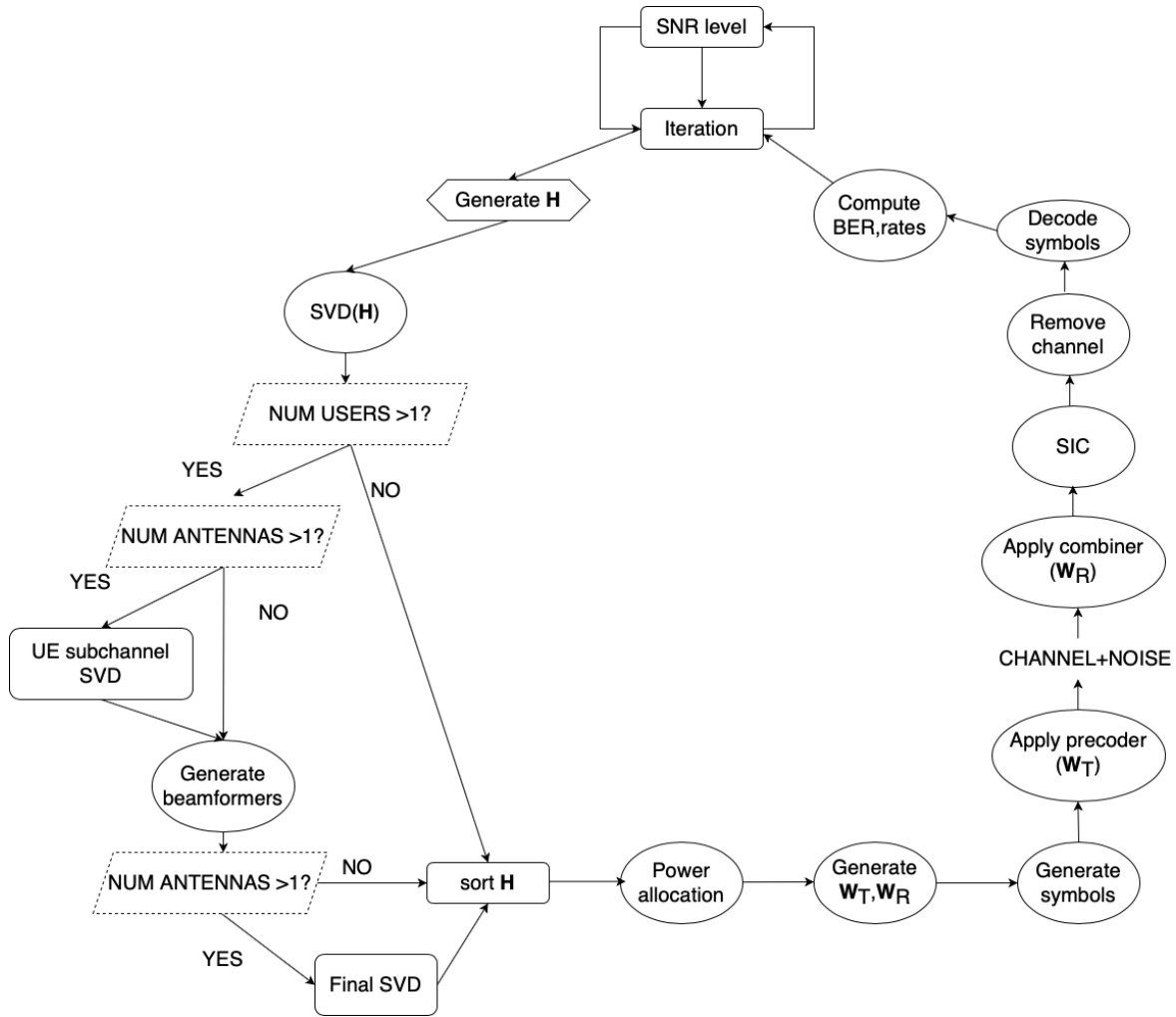


Figure 3.1: Flow chart of the SW

3.2 SISO

3.2.1 Gaussian channel

With the purpose to evaluate the correct implementation of the SW, the Gaussian channel is first evaluated for its simplicity. It does not introduce phase distortion or amplitude modification. For the SISO scenario, matrix \mathbf{H} consists only of one value equal to 1 ($h = 1$). According to [17], the BER for AWGN Channels for BPSK and QPSK modulation is:

$$BER = Q\left(\frac{2Eb}{N_0}\right) \quad (3.1)$$

where Eb stands for bit energy and N_0 the noise power. Figure 3.2 shows the BER for BPSK and QPSK in the AWGN channel with the theoretical approximation in (3.1). As expected both BER curves are the same because the QPSK modulation is formed by two BPSK, one for each I-Q component.

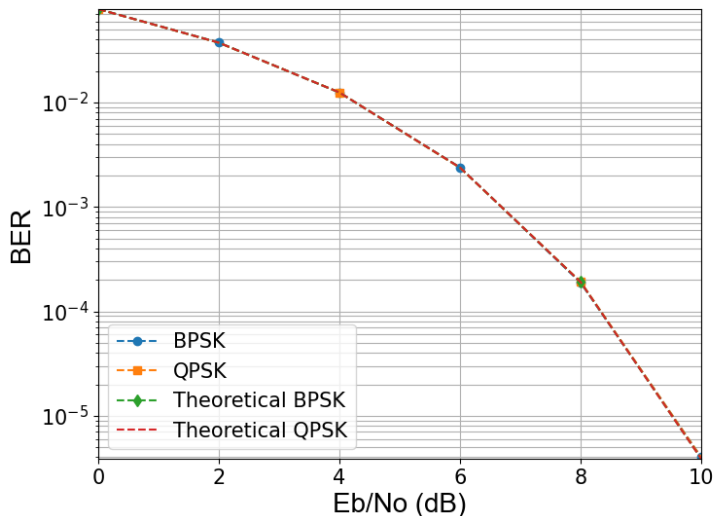


Figure 3.2: BER for SISO in an AWGN channel.

3.2.2 Rayleigh fading channel

The simplest probabilistic model for the channel is to assume that there are many statistically independent reflected and scattered paths with random amplitudes in the delay [15]. The phase of every path is $2\pi f_c \tau_i$, where $f_c \tau_i = d_i/\lambda$ where d_i is the distance traveled by the i -th path and λ the carrier wavelength. Reflectors and scatters can be considered far away compared to the carrier wavelength λ . With that it can be assumed that $d_i \gg \lambda_i$, the phase of each path is uniformly distributed between 0 and 2π and that the phases of the different paths are independent.

According to [15], the contribution of each path at the channel gain can be modeled as a circular symmetric complex random variable. The *circular symmetry* property says that $e^{j\phi}X$ has the same distribution as X for any ϕ .

The real part of the channel gain ($\mathcal{R}(h_l[m])$) is the sum of many small independent random variables and by the Central Limit Theorem (Appendix B) it can be modeled as a zero-mean Gaussian random variable. In addition, because of the uniform phase, ($\mathcal{R}(h_l[m]e^{j\phi})$) is Gaussian with the same variance for any fixed ϕ . This assures that the channel gain is in fact circular symmetric $\mathcal{CN}(0, \sigma_l^2)$. The variance of $h_l[m]$ depends on the l -th tap and for this flat fading case, it is independent of the time instant m .

The scalar complex random variable $h \sim \mathcal{CN}(0, 1)$ has independent identically distributed real and imaginary components each distributed as $\mathcal{N}(0, 1/2)$. The phase of h is uniform between $[0, 2\pi]$ and independent of its magnitude $|h|$, which is Rayleigh distributed, i.e.

$$f(r) = r e^{-\frac{r^2}{2}}, \quad r \geq 0 \quad (3.2)$$

Following the same procedure as in the Gaussian channel, the first test with Rayleigh flat fading channel considers the SISO scenario. Different from the AWGN case, now the channel is not deterministic and it is modeled as a complex normal distribution $h = \mathcal{CN}(0, 1)$. According to the expression in [15], the BER in Rayleigh fading for BPSK constellations is

$$BER = \frac{1}{2} \left(1 - \sqrt{\frac{\rho}{1+\rho}} \right) \quad (3.3)$$

similarly, for QPSK:

$$BER = \frac{1}{2} \left(1 - \sqrt{\frac{\rho}{2+\rho}} \right) \quad (3.4)$$

where ρ is the SNR. In this scenario, it is $\frac{E_s}{N_o}$ where E_s is the symbol energy. In order to compare both constellations and check that the software is properly calibrated, Figure 3.3 depicts the BER for BPSK and QPSK

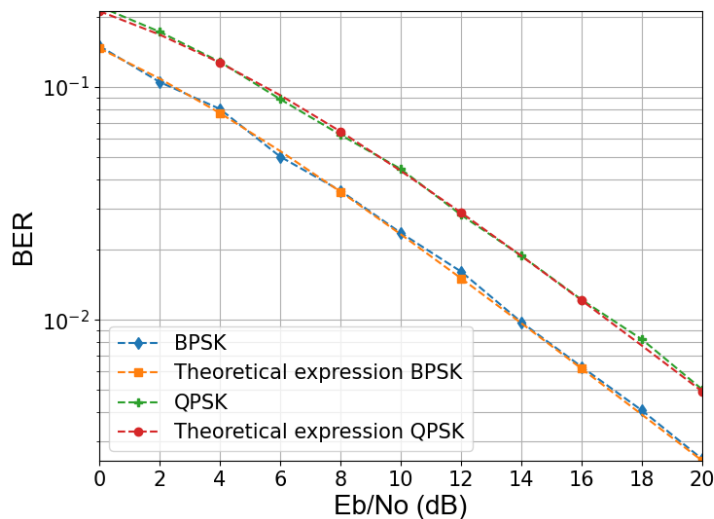


Figure 3.3: BER for SISO in a Rayleigh channel.

3.2.3 Capacity analysis

The received SISO signal for the channel is $y = hx + n$ where n is $\mathcal{CN}(0, N_o)$. As the real and imaginary components are independent, each I-Q component can be considered as $\mathcal{N}(0, \frac{N_o}{2})$. According to [15], the capacity of the channel is

$$C = \frac{1}{2} \log_2(1 + SNR) \quad (3.5)$$

per real dimensions or

$$C = \log_2(1 + SNR) \quad (3.6)$$

per complex dimensions. This presents the upper bound on the number of bits that can be transmitted reliably through this channel with a single channel use. For the AWGN case $h = 1$ and the SNR is simply the ratio between the transmitted signal and the noise: $\frac{P}{N_o}$. Meanwhile, for the Rayleigh channel $h \sim \mathcal{CN}(0, 1)$ and the SNR is $\frac{|h|^2 P}{N_o}$. Figure 3.4 depicts the capacity for the SISO AWGN and Rayleigh channel.

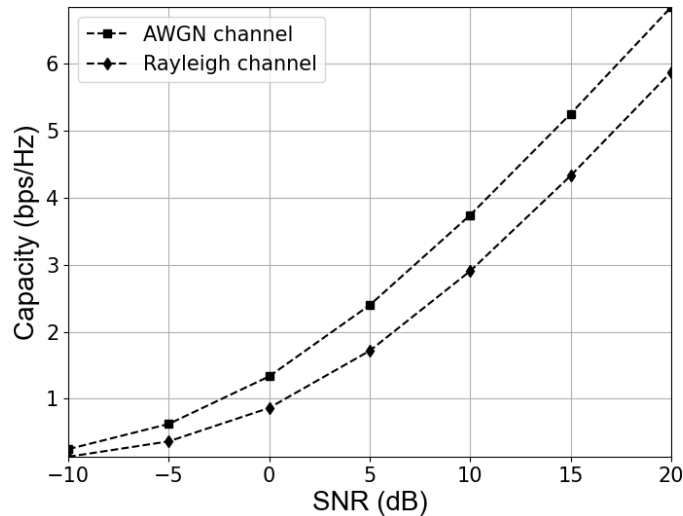


Figure 3.4: Capacity comparison between AWGN and Rayleigh channels.

3.3 MIMO P2P

For the MIMO P2P scenario, the performance is evaluated with two power schemes: UPA and WF algorithm. Figure 3.5 depicts the BER for QPSK modulation with MIMO P2P and two antennas in TX and RX. It is important notice that each curve refers to the information of every stream, which does not mean that it is always attributed to the same physical antenna. Stream 2 possesses the best channel condition compared to stream 1. For that reason, stream 2 has better BER performance than the expressions derived in [15] and stream 1 is worse.

Comparing the two power strategies in Figure 3.5, the BER for the best stream (this is number two) is lower with WF than UPA, but for the second stream, the BER for UPA is slightly better than for WF. This is consistent as WF assigns more power to the best channel (stream 2) and less power to the worst (lower than what UPA would assign).

Another observation is the gain in performance of the WF compared to UPA through the different SNR levels. According to [15], at a high SNR regime, the water level for the WF algorithm is deep and the policy of allocating equal amounts of power is asymptotically optimal.

At a low SNR regime, as the available power is very small, the optimal policy is only to use the strongest eigenvalue. This is the reason why in Figure 3.5 at a high SNR regime the performance of UPA and WF is almost the same. Whereas in low SNR, WF outperforms UPA.

Moving to the analysis of capacity, because our system has full CSI at TX and RX, capacity is computed following Equation (2.14). Analyzing the individual rates of every power strategy in Figure 3.6, the best channel (stream 2) has a higher rate compared to 1.

The sum rate stands for the total rate of the UE, summing every stream rate. For WF, the sum rate is equal to capacity. For UPA, the sum rate achieves capacity at a high SNR regime (it is optimal) and is lower than capacity at low SNR.

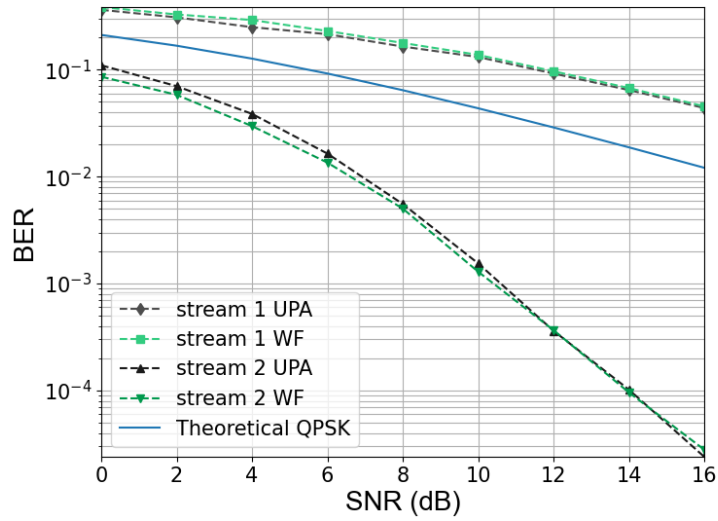


Figure 3.5: MIMO P2P BER for different power allocation strategies.

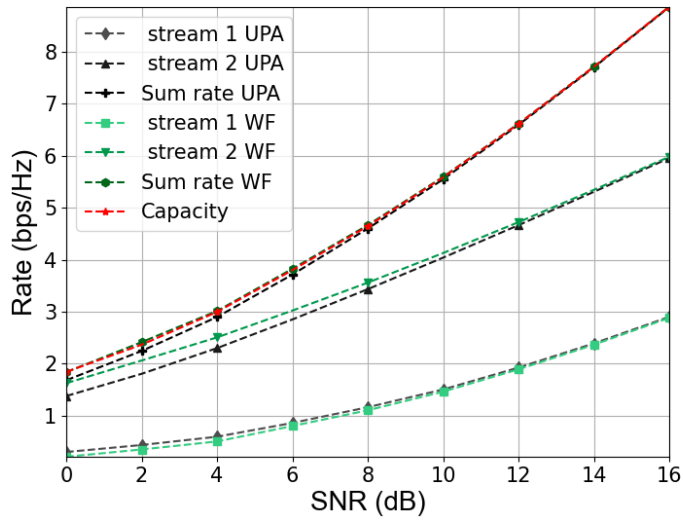


Figure 3.6: Rate analysis for MIMO P2P with different power allocation strategies.

To verify the system, in [15] the capacity is depicted when CSI is available only at the RX for MIMO 4 and 8 antennas with the following expression: $C = \mathbb{E} \left[\log \det \left(\mathbf{I}_{N_R} + \frac{\rho}{N_T} \mathbf{H} \mathbf{H}^H \right) \right]$ which corresponds to the UPA where ρ is the SNR. Figure 3.7 shows the comparison between the curves obtained according to expression from [15] and the simulations using the SW; it can be seen that they match.

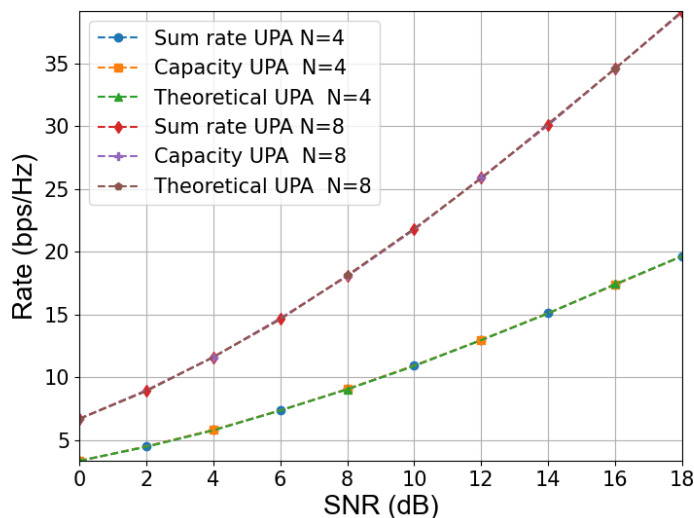


Figure 3.7: Capacity analysis for MIMO P2P with 4 and 8 antennas with UPA. Comparison with the expressions from [15].

3.4 MU-UL with single-antenna UEs

This section analyzes the performance of different beamformers regarding the BER and capacity regions that can be achieved for single-antenna UEs with two power allocation strategies: UPA and WF. Notice that the available power of the system is $\frac{NP}{N_o}$, where N is the number of UEs. In this section, the SNR of the plots refers to the system SNR level. In order to make a proper analysis, first ZF and QR will be studied before moving to the MMSE.

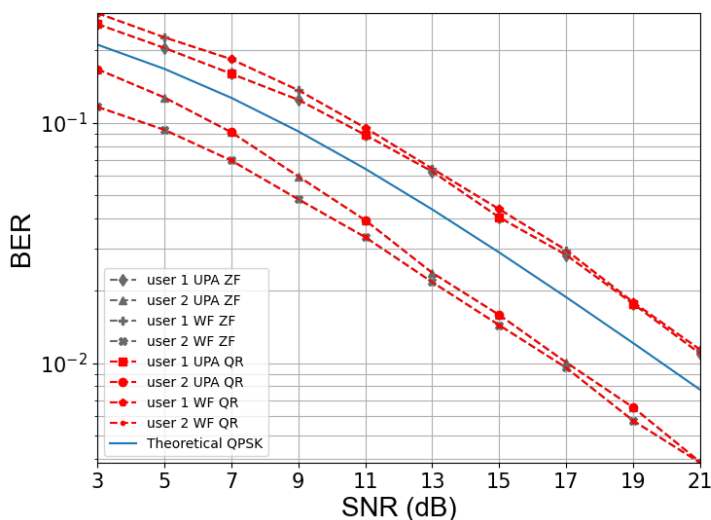


Figure 3.8: BER for two single-antenna UEs using ZF or QR beamformers.

Figure 3.8 depicts the BER for ZF and QR. As explained in Section 2.2, ZF does not tolerate UE interference as the beamformers are orthogonal to channel vectors. QR instead does tolerate some interference in the second UE, but it is removed by SIC. Because of that, the BER performance of both implementations is the same.

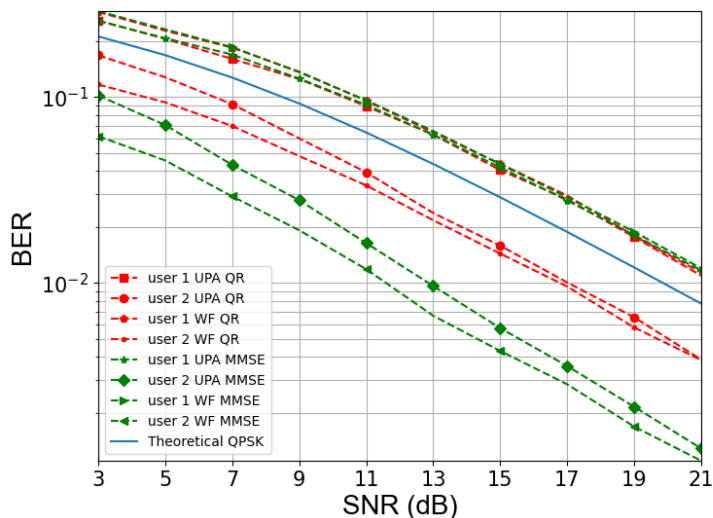


Figure 3.9: BER for two single-antenna UEs using QR or MMSE beamformers.

Although the SNR of Figure 3.8 refers to the global system power, the expression from [15] has been computed with half of this SNR, that is the power devoted to each UE for UPA. With that, the comparison of the different curves can be done.

User 2 has a lower BER than the expression in [15], whereas UE1 surpasses it. The reason is that each UE does not experience the same type of channel because UE2 always has the best channel assigned. Meanwhile, UE1 has the worst. This is not a fair design, but this work aims to reach the maximum sum rate. To do so, UE2 needs to go through the best channel.

Figure 3.9 plots the BER curves for QR and MMSE. Both beamformers are the matched filter for UE1. Therefore the BER curves are equal. Whereas for UE2, MMSE beamformer incorporates the attenuation factor $(\mathbf{I} + E_1 \mathbf{h}_1 \mathbf{h}_1^H)^{-1}$ that nulls the interference of UE1 and the BER is better compared to QR.

Regarding the different power allocation strategies, the curves tend to coincide at a high SNR regime for UE1 and UE2 using the QR. On the contrary, for MMSE the interference that UE2 has to attenuate at a high SNR regime with UPA is higher than in WF so the BER curve for WF performs better.

Moving to the sum rate analysis in Figure 3.10, ZF performs unwell for different SNR levels and MMSE achieves capacity for the whole SNR range. At a high SNR regime, the QR achieves capacity as the noise power is negligible and the MMSE RX does not provide such a large benefit.

Figure 3.11 depicts the capacity and every beamformer's region for an overall system SNR of 3dB and both power allocation schemes. R1 and R2 refer to every UE maximum rate computed as $\log_2(1 + |\mathbf{h}_1|^2 E_1)$ and $\log_2(1 + |\mathbf{h}_2|^2 E_2)$. Red and grey lines represent the capacity region for UPA and WF, respectively.

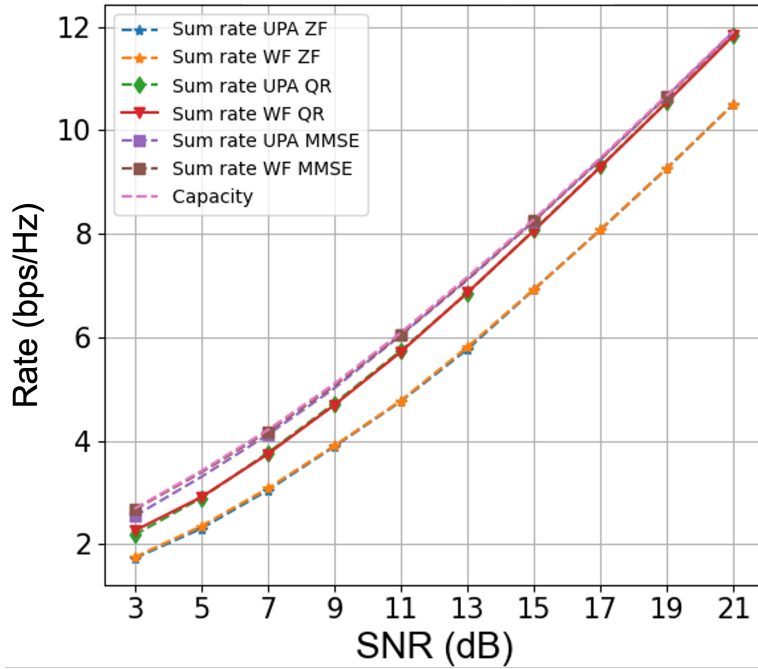


Figure 3.10: Rate analysis for two single-antenna UEs using ZF, QR or MMSE beamformers.

Capacity is computed with the WF algorithm; therefore MMSE beamformer only achieves capacity with WF. The QR region is also a trapezoid because the maximum sum rate is higher than the sum of R_1 max and R_2 max. The maximum sum rate of the ZF is lower than R_1 max and R_2 max, so the region is rectangular. Figure 3.12 analyzes the capacity regions for a higher SNR value which coincide with different power allocations. QR and MMSE regions overlap as QR achieves capacity at a high SNR regime.

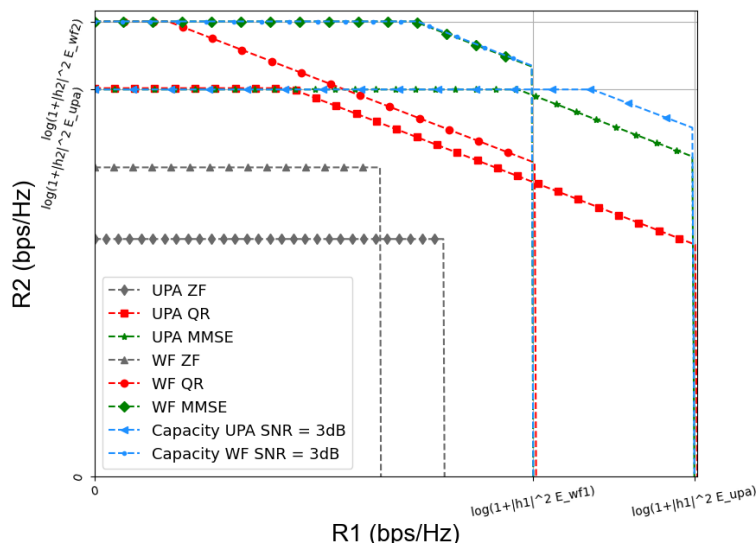


Figure 3.11: Capacity region for MU-UL SNR = 3dB.

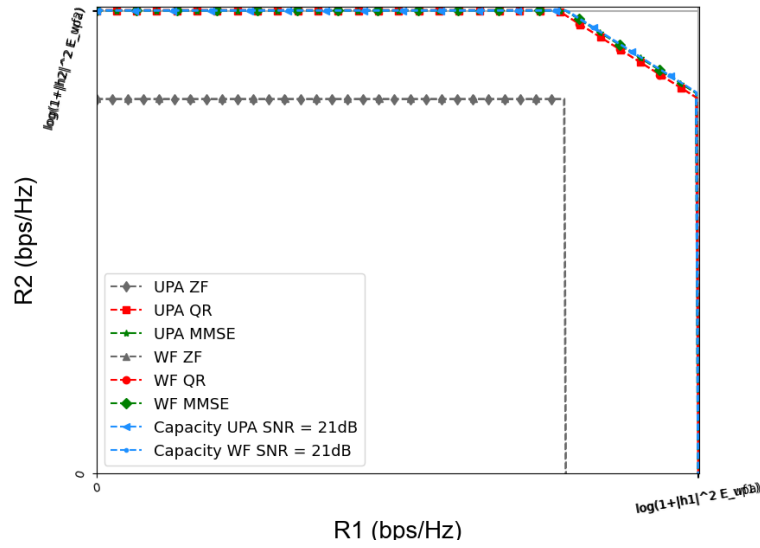


Figure 3.12: Capacity region for MU-UL SNR = 21dB.

3.5 MU-UL with multi-antenna UEs

The optimal power allocation strategy for MU-UL with multi-antenna UEs scenario is that each UE performs WF with his individual channel matrix. The scenario for this section is two UE with two antennas each and a RX with 4. The SNR in the plots refers to the UE SNR (not the overall SNR system) and the expression in [15] is also computed with the UE SNR.

Figure 3.13 shows the BER with the ZF beamformer and QR. Because of the uncorrelated Rayleigh channel, the statistics of each UE's channel matrix are the same and the curves for both UEs are similar. Stream #2 operates better than #1 due to WF. The performance of UE2 for QR and ZF are similar as they are both based on the orthogonal principle. On the contrary, the beamformers of UE1 in QR are the matched filters and their performance is similar to the curves obtained according to the expression from [15]. Stream #2 operates better as he receives more power due to the WF algorithm.

Figure 3.14 depicts the BER plots for the MMSE. The beamformer for UE1 is the matched filter and the curves are parallel to the theoretical expression from [15]. The beamformer for stream #1 of UE2 consists of the attenuation factor and the BER is reduced. The second stream performs badly as the power allocated with the WF is very low.

The overall sum rate for different beamformers is shown in Figure 3.15 where MMSE reaches capacity, QR sum rate is not very far from it and ZF performs unwell. Like the single-antenna case, the capacity region is plotted in Figure 3.16. x -axis contains the overall UE1 rate (sum of two antenna contributions) and y -axis the overall UE2 rate. The region for ZF is rectangular as the maximum sum rate does not reach the sum of the individual maximum rates: $\log_2 (\mathbf{I} + \mathbf{H}_i \mathbf{H}_i^H \mathbf{E}_i)$

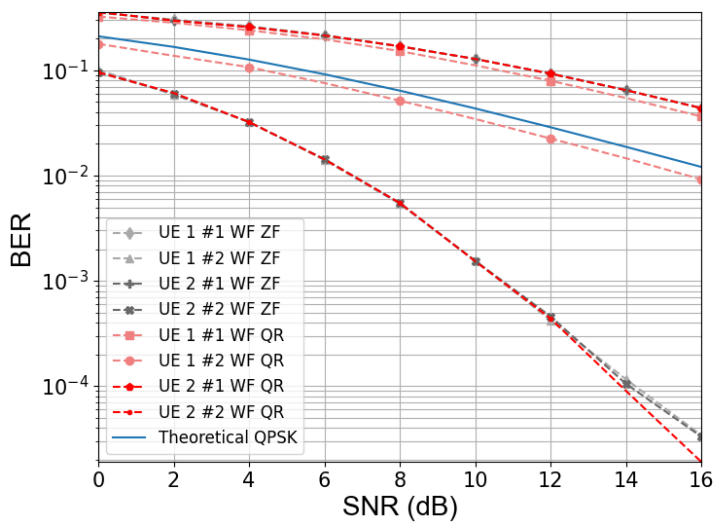


Figure 3.13: BER for ZF and QR.

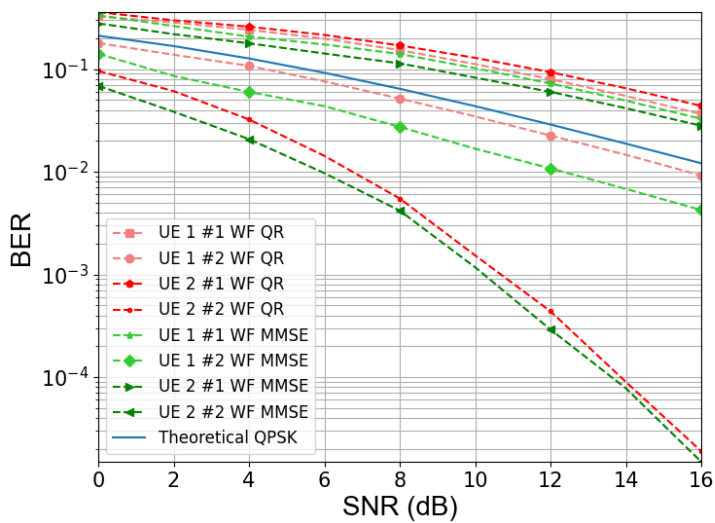


Figure 3.14: BER for QR and MMSE.

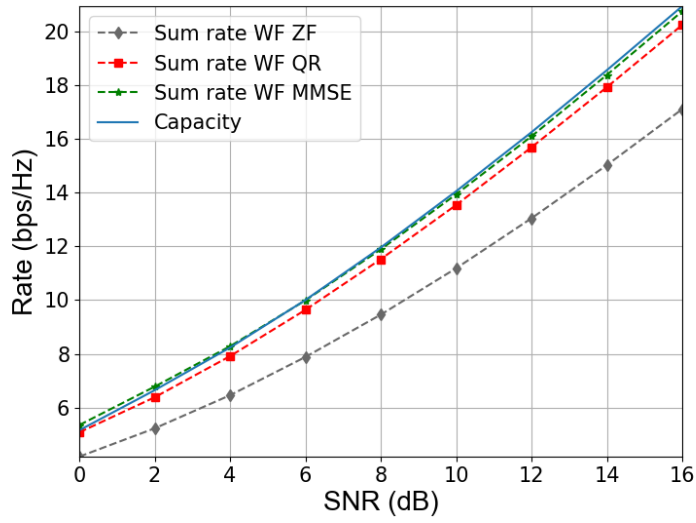


Figure 3.15: Capacity and sum rate analysis for MU-UL.

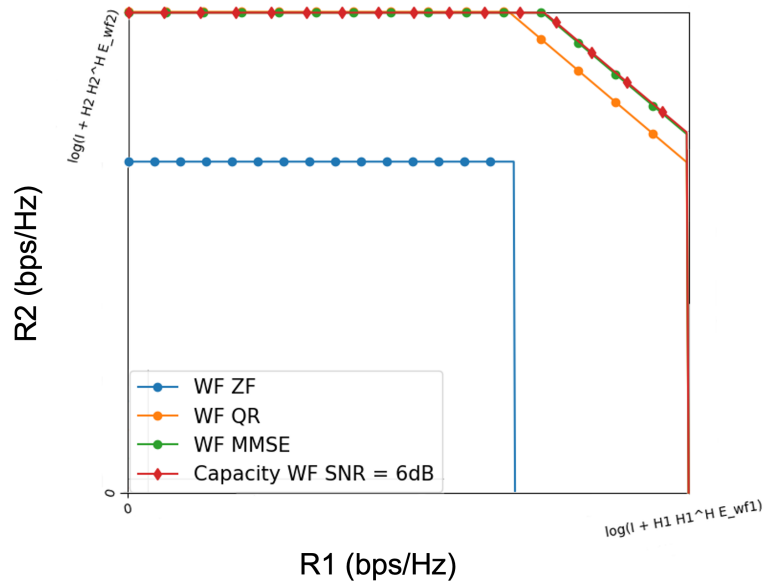


Figure 3.16: Capacity region MU-UL.

4 Channel estimation

The MU-UL design in this thesis requires CSI at both sides of the communication link which means that the RX must estimate the channel and provide its information to the TX by means of a feedback link. In the literature, the CE is done by estimating pilot symbols which are known sequences at both ends of the communication link.

4.1 Pilot symbols transmission

Pilot symbols and feedback channels can be transmitted by two possible modes: Time Division Duplexing (TDD) or Frequency Division Duplexing (FDD). The first requires different time and same frequency resources for UL and DL information. Meanwhile, in FDD pilot symbols are transmitted simultaneously but using different frequency resources.

In the MU-UL MIMO scenario, UL and DL communication are required to satisfy CSI on both sides. This restriction involves channel reciprocity, which means that both transmission directions require the same physical conditions. This requirement is satisfied by TDD mode because UL and DL channels work at the same frequency.

Another element to be decided is who transmits the pilot symbols and performs CE. In UL pilot transmission, each UE needs his time slot to transmit his pilots and the BS needs to estimate every UE channel after his slot. In DL pilot transmission, the pilots are transmitted just once and all UEs can simultaneously estimate the channel. For that reason in several studies such as [18] and [19] DL pilot transmission is preferred.

4.2 Pilot sequence generation for multi-antenna system

Multi-antenna systems make the CE procedure even more difficult since the BS has several antennas and each has to estimate the channel for every TX-RX antenna pair. Different techniques can be adopted in the TX to estimate every channel path properly.

Simultaneous antenna transmissions are preferred in [18] and [19] using orthogonal sequences to properly differentiate the pilot of every antenna as they use the same time and frequency resources. The RX performs correlation for every transmitted pilot sequence and then estimates the channel for every TX-RX antenna pair.

Similar to the 3GPP, this thesis also deals with the simultaneous pilot transmission. The generation of orthogonal sequences is done according to the pseudorandom sequence genera-

tion proposed in 3GPP standards [20]. The reference signal sequence $r(m)$ with length L is defined as:

$$r(m) = \frac{1}{\sqrt{2}}(1 - 2c(2m)) + j\frac{1}{\sqrt{2}}(1 - 2c(2m + 1)) \quad (4.1)$$

The generic pseudo-random sequences are defined by a length-31 Gold sequence. The output $c(n)$ of length $2 * L$ is:

$$c(n) = (x_1(n + N_c) + x_2(n + N_c)) \mod 2 \quad (4.2)$$

$$x_1(n + 31) = (x_1(n + 3) + x_1(n)) \mod 2 \quad (4.3)$$

$$x_2(n + 31) = (x_2(n + 3) + x_2(n + 2) + x_2(n + 1) + x_2(n)) \mod 2 \quad (4.4)$$

where $N_c = 1600$ and the first m-sequence $x_1(n)$ is initialized as

$$x_1(n) = \begin{cases} 1 & \text{if } n = 0 \\ 0 & \text{if } 1 \leq n \leq 30 \end{cases} \quad (4.5)$$

The initialization of the second m-sequence is

$$c_{init} = \sum_{i=0}^{31} x_2(i)2^i \quad (4.6)$$

with the value depending on the application of it. The exact expression for CSI initialization is:

$$c_{init} = (2^{10}(N_{symb}^{slot}n_{s,f}^{\mu} + l + 1)(2n_{ID} + 1) + n_{ID}) \mod 2^{31} \quad (4.7)$$

where N_{symb} , $n_{s,f}$ and n_{ID} are parameters from upper layers. For simplicity, the SW initializes the sequence like this:

$$c_{init} = (2^{10}(8 + i) + 1) \quad (4.8)$$

where i goes from $i_0, \dots, N_T - 1$ for every TX antenna.

TX side

Because of DL pilot transmission, the BS must generate one orthogonal sequence for every antenna. The only difference between sequences is how c_{init} is initialized. Figure 4.1 shows a block diagram of the pilot generation corresponding to a MIMO system with two antennas.

RX side

Every RX antenna needs to estimate the channel for each transmitting one. A block diagram of the RX part is depicted in Figure 4.2. The received symbols at every RX antenna are a combination of pilots from every transmitting one. The channel can be estimated by correlating the RX information with the pilot symbols sequence.

The correlation between sequences x and y is:

$$\hat{R}_{xy}(m) = \begin{cases} \sum_{n=0}^{N-m-1} x_{n+m}y_n^*, & m \geq 0 \\ \hat{R}_{yx}(-m), & m < 0 \end{cases} \quad (4.9)$$

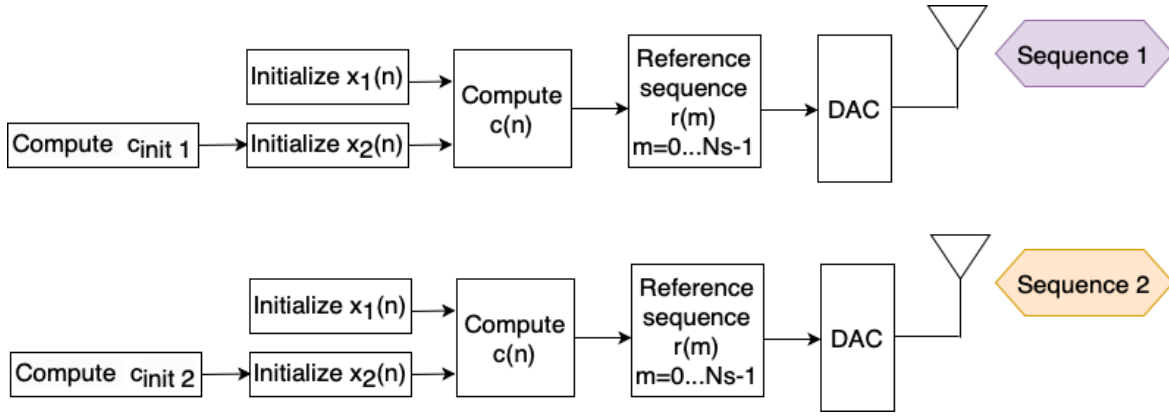


Figure 4.1: Block diagram for Pilot transmission.

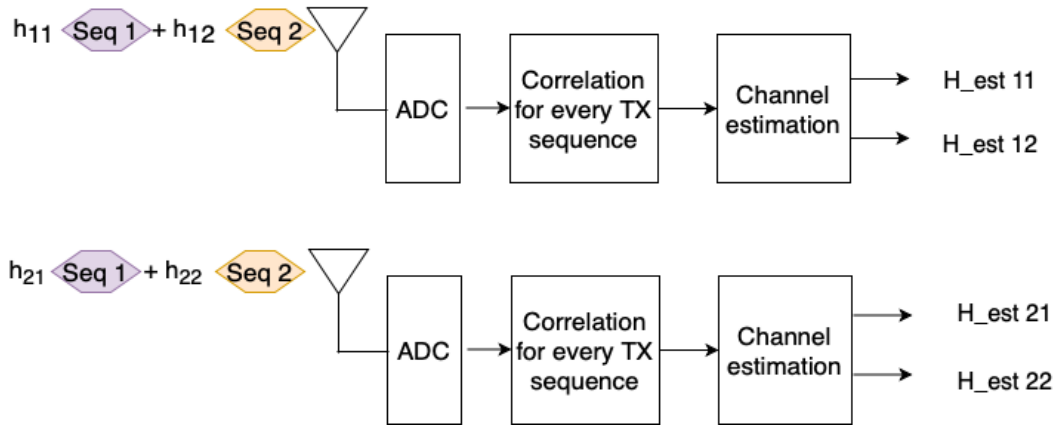
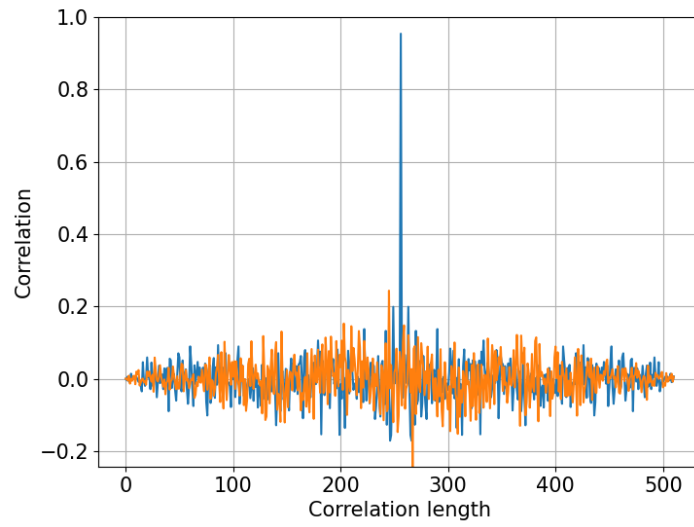


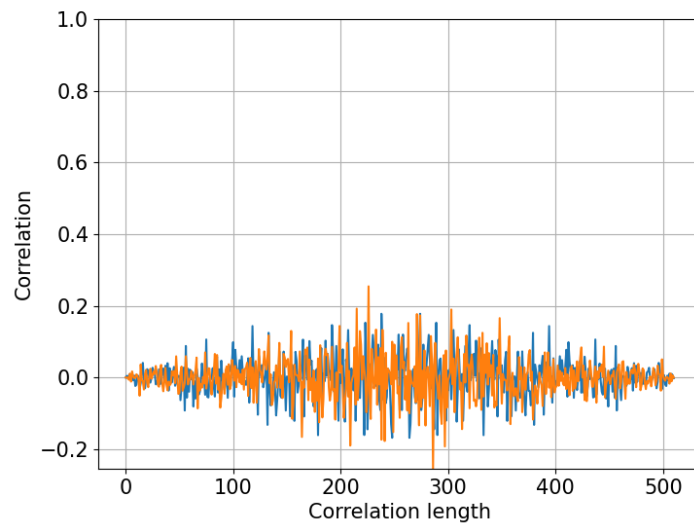
Figure 4.2: Block diagram for Pilot reception and CE.

If both x and y sequences are the same, then the correlation at $m = 0$ is $R_{xx}(0) = LE_s h$ where h is the channel coefficient to be estimated. Therefore the correct estimation is: $\hat{h} = \frac{R_{xx}(0)}{LE_s}$ where E_s is the transmitted power symbol. If x and y are different, as they are designed to be orthogonal, the correlation will be close to 0.

Figure 4.3 shows the correlation normalized to the number of samples (L) for a MIMO 2x2 system when the sequences are the same and orthogonal. The blue and orange lines represent the real and imaginary parts, respectively.



(a) Autocorrelation.



(b) Correlation for orthogonal sequences.

Figure 4.3: Correlation for same and orthogonal sequences.

The quality of the estimator is referred as the Mean Squared Error (MSE) expressed as

$$MSE = (\hat{h}_{est} - h)^2 \quad (4.10)$$

The MSE results for SISO in Figure 4.4 show that MSE reduces as the SNR increases. For the MIMO P2P scenario, the results in Figure 4.5 show the MSE for each of the 2×2 channel matrix entries with N number of pilot symbols. The MSE does not decrease that fast when the SNR increases because the interference between antennas is also higher.

Figures 4.6 and 4.7 show the MSE when using N=128 and N=256 pilot symbols for the MU-UL single and multi-antenna UEs respectively. For single-antenna UEs the MSE is analyzed for each of the 2×2 channel matrix entries and for the multi-antenna scenario, for each of the 4×4 entries. As expected when the number of pilot symbols increases the CE algorithm performs better.

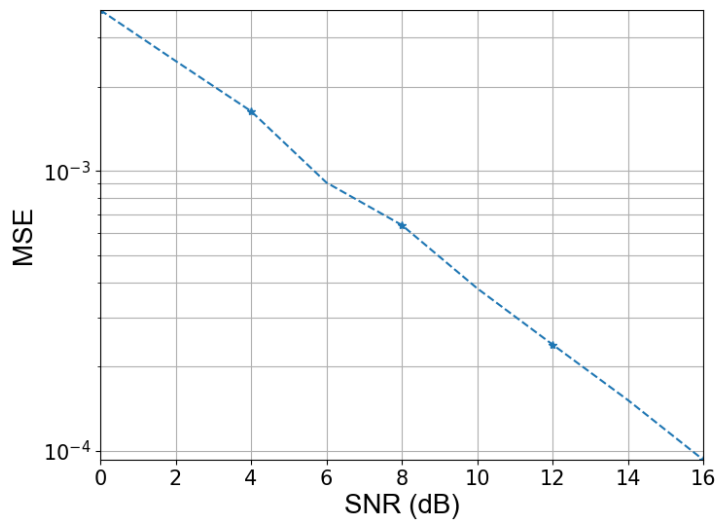


Figure 4.4: MSE for SISO.

Figures 4.8, 4.9 and 4.10 plot the performance comparison in terms of the BER between ideal CSI and with CE for the MIMO P2P, MU-UL with single-antenna UEs and MU-UL with multi-antenna UEs respectively. The BER results are provided for the WF algorithm and a data block with the same size as the number of pilot symbols: N=128 and 256. It is consistent because when the number of pilot symbols increases, the BER decreases and the performance is closer to the ideal channel.

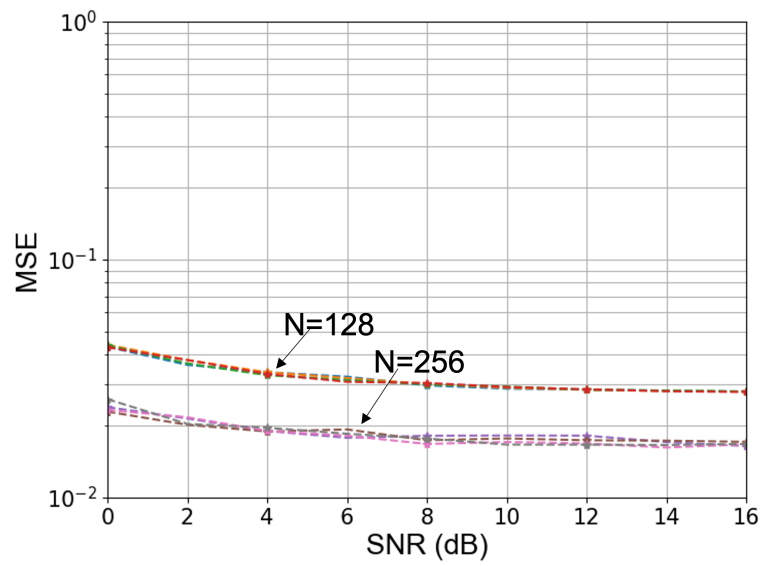


Figure 4.5: MSE for MIMO P2P.

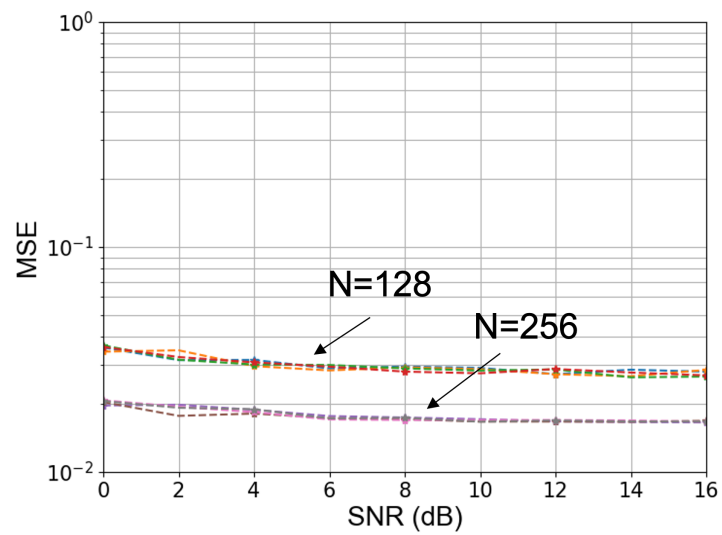


Figure 4.6: MSE for MU-UL with single-antenna UEs.

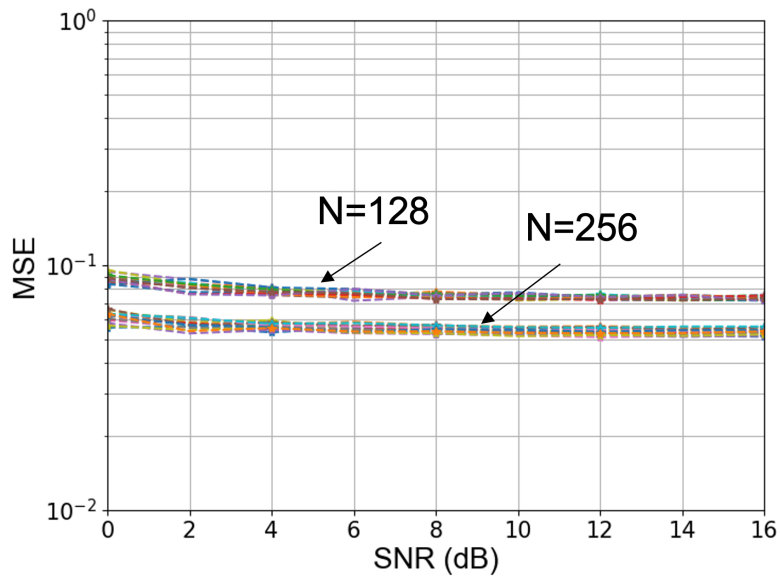


Figure 4.7: MSE for MU-UL with multi-antenna UEs.

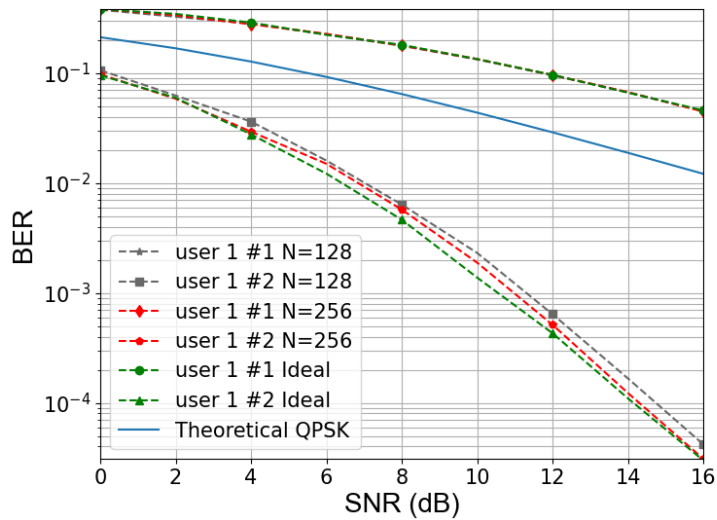


Figure 4.8: BER for MIMO P2P using CE.

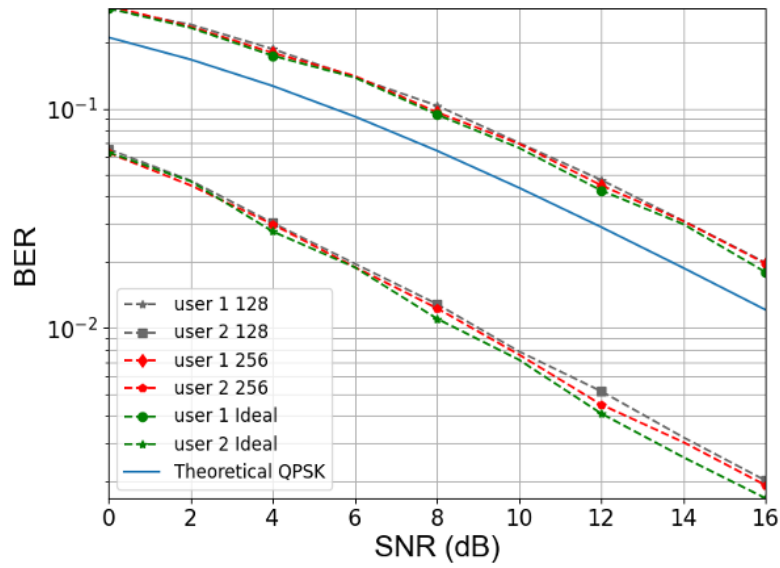


Figure 4.9: BER for MU-UL with single-antenna UEs using CE.

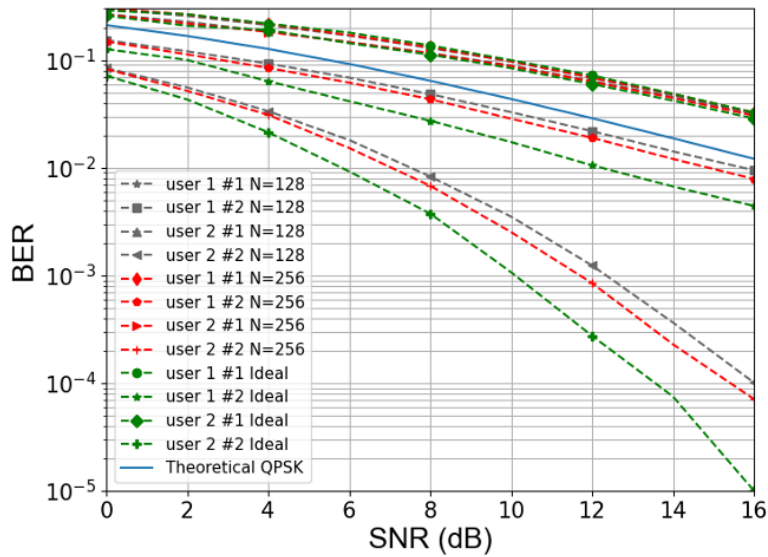


Figure 4.10: BER for MU-UL with multi-antenna UEs using CE.

5 Conclusions

The objective of this thesis was to design the TX and RX for the MU-UL so that it achieves capacity when both ends of the communication channel have CSI. The MU-UL system was simulated in SW and its performance over flat fading Rayleigh channel was evaluated for ZF, QR and MMSE beamformers, and compared against the SISO case.

The performance of the SISO system with BPSK and QPSK modulation schemes is first analyzed with the AWGN channel to serve as a reference. Afterward, the Rayleigh fading channel is introduced and the simulated BER curves coincide with the expressions in [15] for both modulations. For the MIMO P2P systems, the optimal design for the precoder and combiner matrices has been proved to be obtained from the SVD of the channel with WF power allocation. Both UPA and WF power schemes are compared and as expected, both schemes perform equally at a high SNR regime. The trend of the capacity to increase with the number of antennas agrees well with the previous reports in the literature.

Moving on to the MU-UL channel with single-antenna UEs, the optimal design to achieve capacity is the MMSE RX described in Section 2.4.1.4, as it maximizes the SNR and minimizes the MSE in estimating the TX symbols. As derived in Section 2.4.1.5, it acts like a decorrelator or ZF at high SNR, eliminating the interference of other UEs and behaves as a matched filter at low SNR. For a two-UE scenario, the capacity region is trapezoidal and is limited by the maximum individual rates and the capacity of the overall channel matrix. For more than two UEs the capacity region is polyhedral.

Even though the ZF completely removes the interference from other UEs, it is very suboptimal regarding the sum rate for the whole SNR range. The difference between the QR and the MMSE is the maximization SNR term that the latter introduces. At high SNR, the noise level is negligible and both perform the same and achieve capacity.

The final and most complex scenario that gives value to this thesis is the design for the MU-UL with multi-antenna UEs. The optimal TX and RX structures are based on the combined outcomes from MIMO P2P and the MU-UL with single-antenna UEs. The optimal design to achieve capacity is the MMSE RX, with the same fundamentals as for the single-antenna case. The main difference is that instead of dealing with channel vectors, now the beamformers are generated with the channel matrices from every UE. To reach capacity, the optimal power allocation is the WF algorithm with the eigenvalues corresponding to every UE channel matrix.

The goal of this thesis has been accomplished as the sum rate of the designed optimal system has been proved to reach the capacity region for both the MU-UL with single-antenna and multi-antenna UEs. The optimal design in both cases is the RX MMSE and additionally the WF algorithm for the multi-antenna scenario.

The proposed CE method based on orthogonal sequences with an additional feedback channel provides CSI at the RX and TX necessary for the optimal design. The CE algorithm works properly; as when the number of pilot symbols increases, the BER reduces.

Future Works

The proper design for the MU-UL is fundamental to implement more sophisticated schemes for the MU-DL. Existing works in the literature prove that the decentralized architecture at the RX of this MU-DL requires a non-linear precoder. However, in [1], a solution is proposed based on the dual MU-UL to attain the sum capacity.

A clear future line of research of this thesis is the implementation of the optimal TX and RX for the MU-DL system for single and multi-antenna UEs followed by the analysis of its performance. Furthermore, another extension is designing the system from single-carrier to OFDM, which is a more realistic communication approach nowadays.

A SVD decomposition

The theorem considers a matrix A of $m \times n$ dimensions with right singular vectors $\mathbf{v}_1, \mathbf{v}_2, \dots, \mathbf{v}_r$, left singular vectors $\mathbf{u}_1, \mathbf{u}_2, \dots, \mathbf{u}_r$ and corresponding singular values $\sigma_1, \sigma_2, \dots, \sigma_r$. Then

$$\mathbf{A} = \sum_{i=1}^r \sigma_i \mathbf{u}_i \mathbf{v}_i^T \quad (\text{A.1})$$

The decomposition is called the singular value decomposition, SVD, of \mathbf{A} . In matrix notation $A = U\Lambda V^T$ where the columns of U and V consist of the left and right singular vectors respectively and are both unitary matrices, and Λ is a diagonal matrix whose diagonal entries are the singular values of A .

Relation to eigenvalue decomposition The singular value decomposition is very general, since it can be applied to any $m \times n$ matrix whereas the eigenvalue decomposition (EVD) can only be applied to diagonalizable matrices. Nevertheless, the two decompositions are related. Given a SVD of \mathbf{A} , as described above, the following two relations hold:

$$\mathbf{A}^* \mathbf{A} = \mathbf{V} \boldsymbol{\Lambda}^* \mathbf{U}^* \mathbf{U} \boldsymbol{\Lambda} \mathbf{V}^* = \mathbf{V} (\boldsymbol{\Lambda}^* \boldsymbol{\Lambda}) \mathbf{V}^* \quad (\text{A.2})$$

$$\mathbf{A} \mathbf{A}^* = \mathbf{U} \boldsymbol{\Lambda} \mathbf{V}^* \mathbf{V} \boldsymbol{\Lambda}^* \mathbf{U}^* = \mathbf{U} (\boldsymbol{\Lambda} \boldsymbol{\Lambda}^*) \mathbf{U}^* \quad (\text{A.3})$$

During the development of the project, the relation of the SVD and EVD has been exploited since no library which performed SVD with complex numbers was found. Instead of SVD, some libraries had the EVD in complex numbers and permitted to obtain the desired SVD.

B Central Limit Theorem

The Central Limit Theorem (CLT) says that for n independent random variables that are identically distributed with mean equal to μ and finite variance σ^2 . If S_n is the sum of this n random variables $S_n = X_1 + X_2 + \dots + X_n$ and the ratio $\frac{S_n - n\mu}{\sigma\sqrt{n}}$ where $n\mu$ is the mean and $\sigma\sqrt{n}$ the standard deviation of S_n , the CLT points that the distribution of this ratio tends to the normal distribution when n tends to infinity[21]. Which means:

$$P\left(\frac{S_n - n\mu}{\sigma\sqrt{n}} \leq x\right) \xrightarrow{n \rightarrow +\infty} \Phi(x) \quad (\text{B.1})$$

where $\Phi(x)$ is the distribution function of the standard normal distribution expressed by:

$$\Phi(x) = \int_{-\infty}^x \frac{1}{\sqrt{2\pi}} \exp\left(-\frac{x^2}{2}\right) dx \quad (\text{B.2})$$

C Minimum Mean Square Error Estimator

In Equation (2.32) from Section 2.4.1.5, the linear RX that maximizes the SNR is derived. The purpose of this Appendix is to prove that it also minimizes the MSE when the correct factor scaling is used.

To do so, the general channel vector formulation from (2.29) is considered:

$$\mathbf{y} = \mathbf{h}x + \mathbf{z} \quad (\text{C.1})$$

where \mathbf{h} is the deterministic channel vector, \mathbf{z} is $\mathcal{CN}(0, \mathbf{K})$ and x is the zero mean unknown complex random variable to be estimated. The data symbol x and noise \mathbf{z} are assumed to be uncorrelated. The estimate of x is represented as \hat{x} and it is expressed in terms of the RX vector \mathbf{y} , a scaling factor a and a normalized \mathbf{c} vector ($\|\mathbf{c}\| = 1$):

$$\hat{x} = a\mathbf{c}^H\mathbf{y} \quad (\text{C.2})$$

The mean square error (MSE) is expressed as:

$$\begin{aligned} \mathbb{E}[|x - \hat{x}|^2] &= \mathbb{E}[x^2 + \hat{x}^2 - 2x\hat{x}] \\ &= \mathbb{E}[x^2 + a^2|\mathbf{c}^H\mathbf{y}|^2 - 2ax\mathbf{c}^H\mathbf{y}] \end{aligned} \quad (\text{C.3})$$

the factor a that provides the MMSE is calculated by the derivative of the MSE respect to a and equaling to 0:

$$\frac{\partial \text{MSE}}{\partial a} = \mathbb{E}[2a|\mathbf{c}^H\mathbf{y}|^2 - 2x\mathbf{c}^H\mathbf{y}] = 0 \quad (\text{C.4})$$

$$a = \frac{\mathbb{E}[x\mathbf{c}^H\mathbf{y}]}{\mathbb{E}[|\mathbf{c}^H\mathbf{y}|^2]} \quad (\text{C.5})$$

Developing the numerator and denominator:

$$\begin{aligned} \mathbb{E}[x\mathbf{c}^H\mathbf{y}] &= \mathbb{E}[\mathbf{c}^H\mathbf{h}x^2] + \mathbb{E}[x\mathbf{c}^H\mathbf{z}] \\ &= \mathbb{E}[x^2]\mathbf{c}^H\mathbf{h} \end{aligned} \quad (\text{C.6})$$

$$\begin{aligned} \mathbb{E}[|\mathbf{c}^H\mathbf{y}|^2] &= \mathbb{E}[(\mathbf{c}^H(\mathbf{h}x + \mathbf{z}))^2] \\ &= \mathbb{E}[\mathbf{c}^H(\mathbf{h}x + \mathbf{z})(\mathbf{h}x + \mathbf{z})^H\mathbf{c}] \\ &= \mathbb{E}[x^2\mathbf{c}^H\mathbf{h}\mathbf{h}^H\mathbf{c} + \mathbf{c}^H\mathbf{z}\mathbf{z}^H\mathbf{c} + x\mathbf{c}^H\mathbf{h}\mathbf{z}^H\mathbf{c} + x\mathbf{c}^H\mathbf{z}\mathbf{h}^H\mathbf{c}] \\ &= \mathbb{E}[x^2]|\mathbf{c}^H\mathbf{h}|^2 + \mathbf{c}^H\mathbf{K}\mathbf{c} \end{aligned} \quad (\text{C.7})$$

Finally, the constant a that minimizes the MSE ($\mathbb{E}[|x - \hat{x}|^2]$) is

$$a = \frac{\mathbb{E}[|x|^2] \mathbf{c}^H \mathbf{h}}{\mathbb{E}[|x|^2] |\mathbf{c}^H \mathbf{h}|^2 + \mathbf{c}^H \mathbf{K} \mathbf{c}} \quad (\text{C.8})$$

Substituting a to the expression of the MSE in Equation C.4 provides the MMSE that is equal to

$$\begin{aligned} MMSE &= \mathbb{E}[x^2] + a^2 (\mathbf{c}^H \mathbf{K} \mathbf{c} + \mathbb{E}[x^2] |\mathbf{c}^H \mathbf{h}|^2) - 2a \mathbb{E}[x^2] \mathbf{c}^H \mathbf{h} \\ &= \mathbb{E}[x^2] + \frac{(\mathbb{E}[x^2] \mathbf{c}^H \mathbf{h})^2}{\mathbb{E}[x^2] |\mathbf{c}^H \mathbf{h}|^2 + \mathbf{c}^H \mathbf{K} \mathbf{c}} - 2 \frac{(\mathbb{E}[x^2] \mathbf{c}^H \mathbf{h})^2}{\mathbb{E}[x^2] |\mathbf{c}^H \mathbf{h}|^2 + \mathbf{c}^H \mathbf{K} \mathbf{c}} \\ &= \mathbb{E}[x^2] - \frac{(\mathbb{E}[x^2] \mathbf{c}^H \mathbf{h})^2}{\mathbb{E}[x^2] |\mathbf{c}^H \mathbf{h}|^2 + \mathbf{c}^H \mathbf{K} \mathbf{c}} \\ &= \mathbb{E}[x^2] \left(1 - \frac{\mathbb{E}[x^2] |\mathbf{c}^H \mathbf{h}|^2}{\mathbb{E}[x^2] |\mathbf{c}^H \mathbf{h}|^2 + \mathbf{c}^H \mathbf{K} \mathbf{c}} \right) \end{aligned} \quad (\text{C.9})$$

Rearranging the last MMSE expression, it can be written in terms of the SNR:

$$\begin{aligned} \frac{\mathbb{E}[x^2]}{MMSE} &= \frac{\mathbb{E}[x^2] |\mathbf{c}^H \mathbf{h}|^2 + \mathbf{c}^H \mathbf{K} \mathbf{c}}{\mathbf{c}^H \mathbf{K} \mathbf{c}} \\ &= 1 + \frac{\mathbb{E}[x^2] |\mathbf{c}^H \mathbf{h}|^2}{\mathbf{c}^H \mathbf{K} \mathbf{c}} \\ &= 1 + SNR \end{aligned} \quad (\text{C.10})$$

Moving back to Equation (2.32) from Section 2.4.1.5, the \mathbf{c} vector is $\mathbf{c} = \mathbf{K}^{-1} \mathbf{h}$ and with the proper scaling it is the MMSE estimator. The SNR achieved is

$$\begin{aligned} SNR &= \frac{\mathbb{E}[x^2] |\mathbf{c}^H \mathbf{h}|^2}{\mathbf{c}^H \mathbf{K} \mathbf{c}} \\ &= \frac{\mathbb{E}[x^2] \mathbf{h}^H \mathbf{K}^{-1} \mathbf{h}}{\mathbf{h}^H \mathbf{K}^{-1} \mathbf{K} \mathbf{K}^{-1} \mathbf{h}} \\ &= \mathbb{E}[x^2] \mathbf{h}^H \mathbf{K}^{-1} \mathbf{h} \end{aligned} \quad (\text{C.11})$$

D Detection in Gaussian Noise

In order to justify the information lossless property of $I(x; \mathbf{y})$, first the optimal detector in AWGN needs to be explained.

Scalar detection

Considering the RX scalar real signal $y = u + n$ where u is the TX symbol with two possible values u_A and u_B and n the RX AWGN noise distributed as $n \sim \mathcal{N}(0, N_o/2)$. The detection problem reduces to decide for the symbol with highest probability to have been TX. u_A is chosen if

$$\mathbb{P}\{u = u_A | y\} \geq \mathbb{P}\{u = u_B | y\} \quad (\text{D.1})$$

The ML RX chooses the TX symbol that makes the observation y most likely. Conditioned on $u = u_i$, the RX signal y is distributed as $y \sim (u_i, N_o/2)$ where $i = A, B$. The decision rule is to choose u_A if

$$\frac{1}{\sqrt{\pi N_o}} \exp\left(-\frac{(y - u_A)^2}{N_o}\right) \geq \frac{1}{\sqrt{\pi N_o}} \exp\left(-\frac{(y - u_B)^2}{N_o}\right) \quad (\text{D.2})$$

and u_B otherwise. The ML detector in D.1 simplifies to

$$|y - u_A| < |y - u_B| \quad (\text{D.3})$$

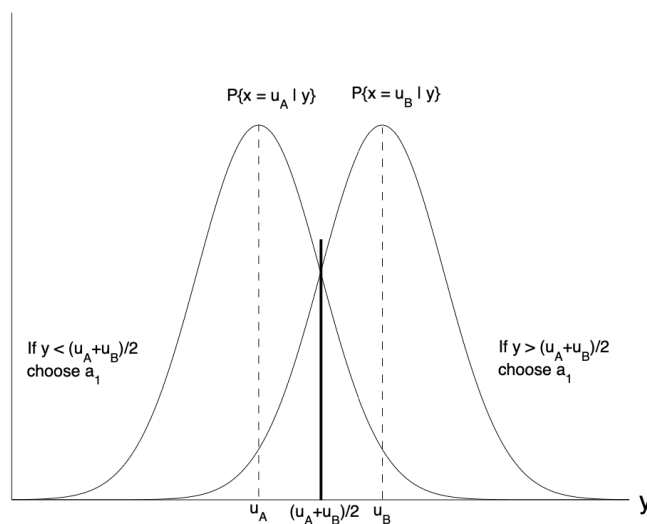


Figure D.1: ML detector

and can be interpreted as if the decision was to decide for the symbol closest to the observation. A visual explanation can be seen in figure D.1. The probability of making an error is

$$\mathbb{P}\left(y < \frac{u_A + u_B}{2} \mid u = u_A\right) = \mathbb{P}\left(n > \frac{|u_A - u_B|}{2}\right) = Q\left(\frac{|u_A - u_B|}{2\sqrt{N_0/2}}\right) \quad (\text{D.4})$$

The error probability only depends on the distance between u_A and u_B .

Detection in Vector Space

If instead of transmitting a scalar symbol u , a real vector \mathbf{u} is TX, the RX signal is

$$\mathbf{y} = \mathbf{u} + \mathbf{n} \quad (\text{D.5})$$

and $\mathbf{n} \sim \mathcal{N}(0, N_0/2\mathbf{I})$. Analogous to D.6, \mathbf{u}_A will be detected if

$$\frac{1}{(\pi N_0)^{n/2}} \exp\left(-\frac{(y - \mathbf{u}_A)^2}{N_0}\right) \geq \frac{1}{(\pi N_0)^{n/2}} \exp\left(-\frac{(y - \mathbf{u}_B)^2}{N_0}\right) \quad (\text{D.6})$$

and can also be simplified to

$$\|\mathbf{y} - \mathbf{u}_A\| < \|\mathbf{y} - \mathbf{u}_B\| \quad (\text{D.7})$$

By the isotropic property of the Gaussian noise, the error probability for every symbol is the same. If symbol \mathbf{u}_A is TX, an error occurs if D.7 does not occur, i.e. $\|\mathbf{w}\| > \|\mathbf{w} + \mathbf{u}_A - \mathbf{u}_B\|$ and the error probability can be expressed as

$$\mathbb{P}(\|\mathbf{w}\|^2 > \|\mathbf{w} + \mathbf{u}_A - \mathbf{u}_B\|^2) = \mathbb{P}\left((\mathbf{u}_A - \mathbf{u}_B)^t \mathbf{w} < -\frac{\|(\mathbf{u}_A - \mathbf{u}_B)\|^2}{2}\right) \quad (\text{D.8})$$

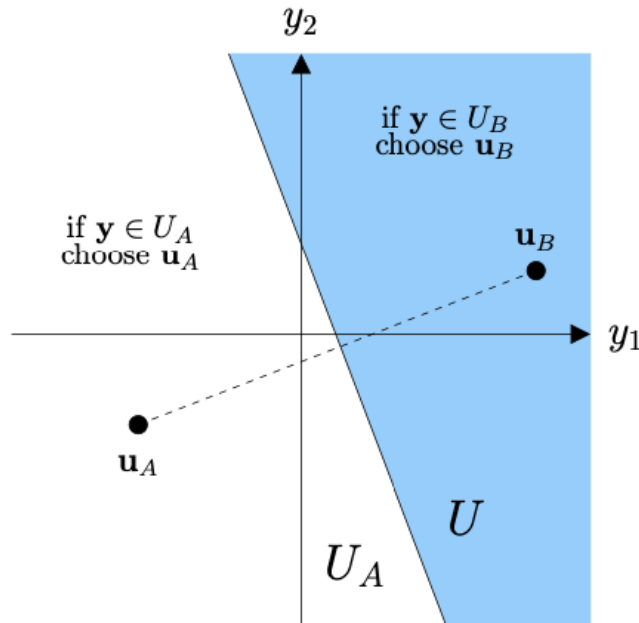


Figure D.2: Decision regions determined by the hyperplane perpendicular to $\mathbf{u}_B - \mathbf{u}_A$

Geometrically, the decision regions are the two sides of the hyperplanes perpendicular to the vector $\mathbf{u}_B - \mathbf{u}_A$ and an error occurs when the RX vector lies on the side of the hyperplane opposite to the TX vector. This can be more clearly seen in Figure D.2.

An Alternative View

The vector detection problem can be seen as a scalar detection one just by changing the way the signal is thought to be transmitted. The TX vector can be seen as

$$\mathbf{u} = x(\mathbf{u}_A - \mathbf{u}_B) + \frac{1}{2}(\mathbf{u}_A + \mathbf{u}_B) \quad (\text{D.9})$$

the information x now is scalar and could be $\pm\frac{1}{2}$. Substituting (D.9) to (D.5) and subtracting $\frac{1}{2}(\mathbf{u}_A + \mathbf{u}_B)$ from \mathbf{y} :

$$\mathbf{y} - \frac{1}{2}(\mathbf{u}_A + \mathbf{u}_B) = x(\mathbf{u}_A - \mathbf{u}_B) + \mathbf{n} \quad (\text{D.10})$$

The TX information x is only in one direction:

$$\mathbf{v} = \frac{(\mathbf{u}_A - \mathbf{u}_B)}{\|\mathbf{u}_A - \mathbf{u}_B\|} \quad (\text{D.11})$$

The components of the RX vector \mathbf{y} in the direction orthogonal to \mathbf{v} contain only noise. Because of the isotropic property of \mathbf{n} , the noise in these directions is also orthogonal to the signal direction and are irrelevant for detection. Therefore projecting the RX signal \mathbf{y} onto the signal direction \mathbf{v} provides all the necessary information for detection:

$$\tilde{y} := \mathbf{v}^t \left(\mathbf{y} - \frac{1}{2}(\mathbf{u}_A + \mathbf{u}_B) \right) \quad (\text{D.12})$$

Figure D.3 offers a visual representation for the projection of the RX signal \mathbf{y} onto the signal

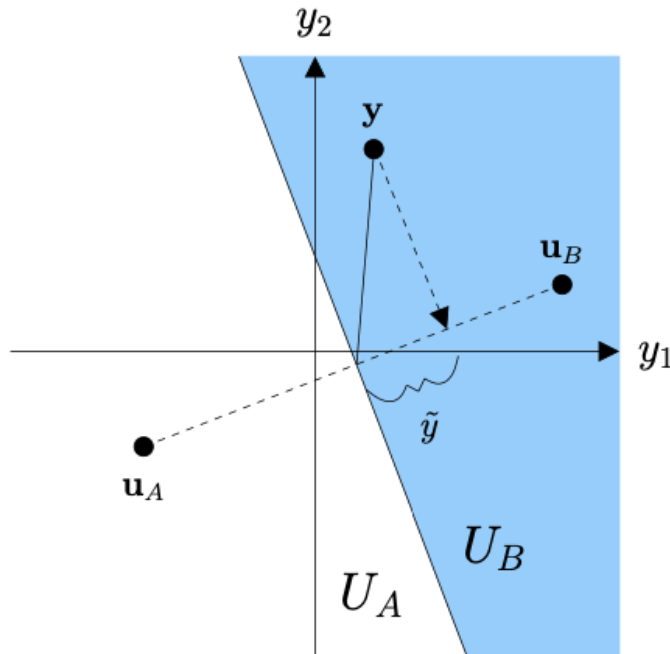


Figure D.3: Projection of \mathbf{y} onto the signal direction \mathbf{v} .

direction \mathbf{v} , reducing the vector detection problem to a scalar one. Considering the error probability in (D.4), now for the vector detection case is

$$Q \left(\frac{|\mathbf{u}_A - \mathbf{u}_B|}{2\sqrt{N_0/2}} \right) \quad (\text{D.13})$$

Up to now, the detection problem is binary as the number of possible TX symbols is 2. To generalize it for M vectors $\mathbf{u}_1, \dots, \mathbf{u}_M$, the projection of \mathbf{y} onto the subspace spanned by $\mathbf{u}_1, \dots, \mathbf{u}_M$ is a sufficient statistic for the detection problem. If the vectors \mathbf{u}_i are collinear, i.e. $\mathbf{u}_i = \mathbf{h}_i x$ for some vector \mathbf{h} , a projection onto the direction of \mathbf{h} provides a sufficient statistic.

Detection in a Complex Vector Space

Reformulating expression (D.5) for the complex scenario

$$\mathbf{y} = \mathbf{u} + \mathbf{n} \quad (\text{D.14})$$

now \mathbf{n} is distributed as $\mathbf{n} \sim \mathcal{CN}(0, N_0 \mathbf{I})$. Rewriting \mathbf{u} as in the real case

$$\mathbf{u} = x(\mathbf{u}_A - \mathbf{u}_B) + \frac{1}{2}(\mathbf{u}_A + \mathbf{u}_B) \quad (\text{D.15})$$

The signal in this direction is

$$\mathbf{v} = \frac{(\mathbf{u}_A - \mathbf{u}_B)}{\|\mathbf{u}_A - \mathbf{u}_B\|} \quad (\text{D.16})$$

The projection of the RX vector \mathbf{y} onto \mathbf{v} provides a complex scalar sufficient statistic:

$$\tilde{y} := \mathbf{v}^* \left(\mathbf{y} - \frac{1}{2}(\mathbf{u}_A + \mathbf{u}_B) \right) = x \|\mathbf{u}_A - \mathbf{u}_B\| + n \quad (\text{D.17})$$

where $n \sim \mathcal{CN}(0, N_0)$. Since x is real ($\pm 1/2$), the sufficient statistic is extracted just by looking at the real component

$$\mathbb{R}[\tilde{y}] = x \|\mathbf{u}_A - \mathbf{u}_B\| + \mathbb{R}[n] \quad (\text{D.18})$$

where $\mathbb{R}[n] \sim N(0, N_0/2)$. The probability of error is the same as in (D.13)

$$Q \left(\frac{\|\mathbf{u}_A - \mathbf{u}_B\|}{2\sqrt{N_0/2}} \right) \quad (\text{D.19})$$

In this example, even if vectors \mathbf{u}_A and \mathbf{u}_B are complex, the detection problem can be seen just in one real dimension as the number of possible symbols is 2:

$$x(\mathbf{u}_A - \mathbf{u}_B) + \frac{1}{2}(\mathbf{u}_A + \mathbf{u}_B) \quad (\text{D.20})$$

If the number of possible symbols is larger, $\mathbf{h}x_i$ where x_i is complex, $\mathbf{h}^* \mathbf{y}$ is still a sufficient statistic but $\mathbb{R}[\mathbf{h}^* \mathbf{y}]$ is sufficient only if x is real.

To summarize, for collinear signals (for example the ones in Pulse-Amplitude Modulation constellations), the RX vector can be expressed as

$$\mathbf{y} = \mathbf{h}x + \mathbf{n} \quad (\text{D.21})$$

where x takes values in the finite set of the constellation points \mathcal{C} and \mathbf{h} has a fixed value. Projecting \mathbf{y} onto the unit vector $\mathbf{v} := \frac{\mathbf{h}}{\|\mathbf{h}\|}$ yields a scalar sufficient statistic

$$\mathbf{v}^* \mathbf{y} = \|\mathbf{h}\|x + n \quad (\text{D.22})$$

where $n \sim \mathcal{CN}(0, N_0)$

List of Figures

2.1	SISO.	7
2.2	SIMO.	7
2.3	MISO.	7
2.4	MIMO.	8
2.5	Schematic of the power filling algorithm.	10
2.6	P2P Virtual links.	10
2.7	Equivalent channel.	11
2.8	System model for MU-UL single-antenna UEs.	11
2.9	System model for MU-UL multi-antenna UEs.	12
2.10	MU-UL Capacity region for two UEs.	13
2.11	MU-UL Capacity region for two UEs with independent decoding at the RX.	14
2.12	MU-UL single-antenna UEs.	14
2.13	Schematic representation of the projection operation.	15
2.14	SIC for three UEs.	16
2.15	Optimal filter that goes from ZF at high SNR to the Matched Filter at low SNR.	18
2.16	Comparison of the rate-capacity ratio of different RXs.	19
2.17	MMSE-SIC achieves capacity for an i.i.d. Rayleigh fading channel.	20
2.18	MU-UL multi-antenna UEs.	21
2.19	Capacity region for two multi-antennas UEs.	22
2.20	TX block MU-UL channel with multiple antennas.	22
2.21	Complete TX and RX chain.	25
3.1	Flow chart of the SW	28
3.2	BER for SISO in an AWGN channel.	29
3.3	BER for SISO in a Rayleigh channel.	30
3.4	Capacity comparison between AWGN and Rayleigh channels.	31
3.5	MIMO P2P BER for different power allocation strategies.	32
3.6	Rate analysis for MIMO P2P with different power allocation strategies.	32
3.7	Capacity analysis for MIMO P2P with 4 and 8 antennas with UPA. Comparison with the expressions from [15].	33
3.8	BER for two single-antenna UEs using ZF or QR beamformers.	33
3.9	BER for two single-antenna UEs using QR or MMSE beamformers.	34

3.10	Rate analysis for two single-antenna UEs using ZF, QR or MMSE beamformers.	35
3.11	Capacity region for MU-UL SNR = 3dB.	35
3.12	Capacity region for MU-UL SNR = 21dB.	36
3.13	BER for ZF and QR.	37
3.14	BER for QR and MMSE.	37
3.15	Capacity and sum rate analysis for MU-UL.	38
3.16	Capacity region MU-UL.	38
4.1	Block diagram for Pilot transmission.	41
4.2	Block diagram for Pilot reception and CE.	41
4.3	Correlation for same and orthogonal sequences.	42
4.4	MSE for SISO.	43
4.5	MSE for MIMO P2P.	44
4.6	MSE for MU-UL with single-antenna UEs.	44
4.7	MSE for MU-UL with multi-antenna UEs.	45
4.8	BER for MIMO P2P using CE.	45
4.9	BER for MU-UL with single-antenna UEs using CE.	46
4.10	BER for MU-UL with multi-antenna UEs using CE.	46
D.1	ML detector	55
D.2	Decision regions determined by the hyperplane perpendicular to $\mathbf{u}_B - \mathbf{u}_A$	56
D.3	Projection of \mathbf{y} onto the signal direction \mathbf{v} .	57

References

- [1] M. L. A. Pérez-Neira, “A new strategy to design and implement the optimal multi-antenna broadcast channel precoder,” in *Proc. 26th International Conference on Circuits, Systems, Communications and Computers (CSCC)*, 2022.
- [2] G. J. Foschini, “Layered space-time architecture for wireless communication in a fading environment when using multi-element antennas,” *Bell Labs Technical Journal*, vol. 1, no. 2, pp. 41–59, 1996.
- [3] Claude E. Shannon, “Two-way Communication Channels,” in *Proc. 4th Berkeley Symposium Mathematical Statistics and Probability (BSMSP)*, vol. 1, Jan 1961, pp. 611–644.
- [4] T. Cover, “Broadcast channels,” *IEEE Transactions on Information Theory*, vol. 18, no. 1, pp. 2–14, Jan 1972.
- [5] N. Jindal, “Multi-user communication systems: Capacity, duality, and cooperation,” Ph.D. dissertation, Stanford University, Jul 2004.
- [6] A. Khina, Y. Kochman, and U. Erez, “The Dirty MIMO Multiple-Access Channel,” in *Proc. IEEE International Symposium on Information Theory (ISIT)*, Jun 2016.
- [7] B. Clerckx and C. Oestges, *MIMO Wireless Networks*, 2nd ed. New Delhi, India: Academic Press, 2013.
- [8] L. Lee, J. Wang, and X. Wu, “ZF beamforming performance analysis for Multi-User spatial multiplexing with imperfect channel feedback,” in *Proc. IEEE International Conference on Wireless Communications, Networking and Mobile Computing (WiCom)*, 2007.
- [9] C.-C. Hu and C.-L. Yang, “Combined transceiver optimization for uplink multiuser MIMO with limited CSI,” *International Scholarly Research Notices*, 2011.
- [10] K. Vehkalahti, “Performance Analysis of Multi-User Massive MIMO Systems with Perfect and Imperfect CSI,” *Procedia Computer Science*, vol. 167, pp. 1452–1461, 2020.
- [11] B. P. Patil, R. Patil, and P. Kavipriya, “Performance Analysis of 8 X 8 MU-MIMO in Uplink of LTE-A,” *International Journal on Emerging Technologies*, 2019.
- [12] H. Q. Ngo, T. Q. Duong, and E. G. Larsson, “Uplink performance analysis of multi-cell MU-MIMO with Zero-Forcing receivers and perfect CSI,” in *Proc. IEEE Swedish Communication Technologies Workshop (Swe-CTW)*, 2011, pp. 40–45.
- [13] A. Paulraj, R. Nabar, and D. Gore, *Introduction to Space-Time Wireless Communications*. New York, NY, USA: Cambridge University Press, 2008.
- [14] B. Suard, Guanghan Xu, Hui Liu, and T. Kailath, “Uplink channel capacity of space-division-multiple-access schemes,” *IEEE Transactions on Information Theory*, vol. 44, no. 4, pp. 1468–1476, 1998.
- [15] D. Tse and P. Viswanath, *Fundamentals of Wireless Communication*. New York, NY, USA: Cambridge Univ. Press, 2005.

- [16] E. W. Weisstein, “QR Decomposition [Online],” 2022, Nov. Available:<https://mathworld.wolfram.com/QRDecomposition.html>
- [17] A. Goldsmith, *Wireless Communications*. New York, NY, USA: Cambridge University Press, 2005.
- [18] Q. Qin, L. Gui, P. Cheng, and B. Gong, “Time-Varying Channel Estimation for Millimeter Wave Multiuser MIMO Systems,” *IEEE Transactions on Vehicular Technology*, vol. 67, no. 10, pp. 9435–9448, 2018.
- [19] Y. Liu, Z. Tan, H. Hu, L. J. Cimini, and G. Y. Li, “Channel Estimation for OFDM,” *IEEE Communications Surveys & Tutorials*, vol. 16, no. 4, pp. 1891–1908, 2014.
- [20] 3GPP, “Physical channels and modulation: Technical Specification (TS).”
- [21] K. Vehkalahti, *The Concise Encyclopedia of Statistics*. Berlin, Germany: Springer, Dec 2007.